Nonlinear Pitch Angle Scattering of Energetic Electrons by Coherent VLF Waves in the Magnetosphere

U. S. INAN, T. F. BELL, AND R. A. HELLIWELL

Radioscience Laboratory, Stanford University, Stanford, California 94305

A computer simulation approach is used to study the nonlinear cyclotron resonant interaction of energetic electrons and coherent VLF waves, with special emphasis on the pitch angle scattering of the particles. Complete equations of motion in an inhomogeneous magnetosphere are used, and the effects of various parameters are studied. Comparison is made with linear theory, and a quantitative and easy-to-use criterion to determine the applicability of linear theory under any given conditions is presented. For example, in the case of equatorial scattering by a 5-kHz CW pulse near $L = 4$ it is found that linear theory begins to break down when the wave amplitude exceeds 3 mγ. The full distribution of particles is simulated by test electrons appropriately distributed in energy and pitch angle. By computing the scattering of these test particles and integrating over energy and pitch angle, the precipitated flux is obtained. The method used is quite general and can be used for any particle distribution. It is shown that significant particle fluxes are precipitated by waves of moderate intensity. For instance, energetic (1–2 keV) electron fluxes as high as $\sim 10^{-1}$ erg/cm^2 s can be precipitated by a CW wave of 10-mγ amplitude and 5-kHz frequency on the $L \simeq 4$ field lines. Such fluxes appear to be measurable with presently available instruments. Since the energy density of the precipitated flux is 50 dB above that of the wave, the leverage involved in the wave-induced precipitation process is quite high. Our results indicate that coherent VLF waves can have a significant effect on the dynamics and lifetimes of energetic electrons trapped in the magnetosphere on magnetic shells illuminated by the waves.

1. INTRODUCTION

This paper presents a study of the nonlinear cyclotron resonance wave-particle interaction in the magnetosphere. In particular, we consider the pitch angle scattering of energetic electrons by coherent VLF whistler mode signals. However, the results and the presentation also clarify many general aspects of the interaction.

There has been considerable work done on the pitch angle scattering of radiation belt particles by electromagnetic waves [*Roberts*, 1966, 1968, 1969; *Dungey*, 1963, 1964; *Gendrin*, 1968; *Kennel and Petschek*, 1966; *Ashour-Abdalla*, 1972; *Kennel and Engelmann*, 1966; *Kennel*, 1969; *Lyons*, 1973, 1974*a*, *b*; *Lyons et al.*, 1971, 1972; *Schulz and Lanzerotti*, 1973]. Most of this work, however, has addressed the problem of scattering by wide band incoherent whistler mode turbulence. The idea has been that the trapped particle population interacts through cyclotron resonance with electromagnetic disturbances along its orbit and is subjected to a series of scatterings that are random in both direction and size. Hence the individual particles of the population undergo a random walk in pitch angle, and diffusion in equatorial pitch angle space results. This diffusion can then be studied by calculating the incoherent diffusion coefficients and solving a Fokker-Planck equation [*Roberts*, 1966].

This approach is well justified for studying particle scattering by certain kinds of magnetospheric signals, for example, auroral VLF hiss or ELF plasmaspheric hiss, since such waves are indeed wide band and highly incoherent [*Muzzio*, 1971; *Gurnett and Frank*, 1972; *Thorne et al.*, 1973; *Laaspere and Hoffman*, 1976].

The physics in our case is fundamentally different because it involves highly coherent narrow band whistler mode waves. When a particle population encounters such coherent waves, the series of scatterings experienced by the particles is not random in direction or size. The individual particles of the population can be phase locked with the coherent signal for distances of many hundred wavelengths and undergo large net pitch angle changes in a single encounter with the wave. It is therefore incorrect to assume that the particles execute a random walk in pitch angle during the course of one bounce period when interacting with coherent waves.

The study of wave-particle interactions with coherent waves is very important. Examples of highly coherent magnetospheric signals are natural whistlers [*Helliwell*, 1965], triggered VLF emissions [*Stiles and Helliwell*, 1975], signals that are injected into the magnetosphere by VLF ground transmitters [*Helliwell and Katsufrakis*, 1974] and large-scale power grids [*Helliwell et al.*, 1975; *Park*, 1976], or signals from satellite-borne VLF transmitters, such as the transmitter planned for the Atmospheric and Magnetospheric Plasmas in Space mission.

During the past three years, VLF wave injection experiments to study coherent VLF wave-particle interactions in the magnetosphere have been carried out with the Stanford University variable frequency VLF transmitter at Siple Station in the Antarctic [*Helliwell and Katsufrakis*, 1974]. One goal of these experiments is to understand the mechanism of wave growth. Another is to learn how to control the energetic particles by the injected waves. The latter problem is the subject of this paper.

Once control is established, the energetic particles can be used as tools to study other important processes. For example, the control of energetic particle precipitation would permit controlled studies of X ray, ionization, and radiation emission processes in the ionosphere. Furthermore, modulation of precipitation flux might provide a means to produce Pc 1 ULF waves [*Bell*, 1976] on a controlled basis. Reducing the particle population in the radiation belts with appropriate transmissions is another possible future application. Although ground transmitters illuminate a relatively large region of the magnetosphere [*Inan et al.*, 1977], satellite transmitters may be necessary for applications requiring high wave amplitudes.

Theoretical studies of the coherent cyclotron resonance wave-particle interaction have concentrated on wave growth and generation due to the phase bunching of the energetic

Paper number 8A0076.
0148-0227/78/078A-0076$01.00

particles [*Brice*, 1964; *Bell and Buneman*, 1964; *Helliwell*, 1967, 1970; *Dysthe*, 1971; *Nunn*, 1971, 1974; *Palmadesso and Schmidt*, 1971, 1972; *Matsumoto*, 1972; *Brinca*, 1972; *Bud'ko et al.*, 1972; *Helliwell and Crystal*, 1973; *Karpman et al.*, 1974*a*, *b*].

Pitch angle scattering induced by coherent waves has been considered by only a few authors. *Gendrin* [1974] has computed the pitch angle and energy perturbations of single particles in a homogeneous medium. *Das* [1971] and *Ashour-Abdalla* [1972] have included the effect of the inhomogeneity but have employed a linear theory in the solution of the motion equations. Although it is generally accepted that linear theory applies for small wave amplitudes, past workers have given no quantitative justification for the assumptions. The main advantage of linear theory is that it considerably simplifies the analysis.

In our approach we have employed a straightforward formulation involving a test particle simulation using the nonlinear equations of motion for energetic electrons in a whistler mode wave in an inhomogeneous magnetosphere. In this approach the effect of the signal on a particle population is calculated by simulating the interaction for a sufficient number of test particles. Each particle is considered independently of the others, allowing sequential rather than parallel computation of the particle trajectories. Although the purpose of this simulation is to compute the wave's effect on the particles, our results are also directly applicable to the problem of wave growth and generation through phase bunching [*Helliwell*, 1967], since we compute the full phase motion of the particles in order to obtain the total scattering.

Since we use a test particle approach, our calculations do not directly include the effects of the electromagnetic fields generated by the perturbed energetic particles. In effect, we assume either that the currents stimulated in the energetic particle population do not lead to significant damping or amplification of the wave or that this effect has been included in the model chosen for the wave field structure. A discussion of this point is included in the final section of this paper.

In this report we have considered two cases of a monochromatic whistler model signal, one in which the wave signal is of constant intensity over the entire field line and one in which the wave signal is of constant intensity over one half of a magnetic field line. The case of a single frequency is not as limiting as it might seem, since there is some reason to believe that the interaction with a wave with linearly increasing or decreasing frequency is quantitatively not much different [*Helliwell*, 1970]. We also limit ourselves to wave propagation strictly along the static magnetic field lines with $\mathbf{k}$ parallel to $\mathbf{B}_0$.

The energy scattering of each test particle can be computed together with its pitch angle scattering. However, herein we have limited our discussion to pitch angle scattering. For most of the particles involved in our calculations the energy scattering is less than $\simeq 2\%$, whereas pitch angle scattering is at times as high as 90%. We have included some brief comments on energy scattering in the figure captions.

In the next section we give a formal description of the problem. We then describe the computer simulation. After that we present and discuss the results for the pitch angle scattering of single particles primarily for the purpose of demonstrating the influence of different parameters. Finally, we give a computation of the precipitated electron flux for a particular case, from a full distribution of energetic electrons.

Our results clearly show the relationships between the total scattering and the various wave, medium, and particle parameters. For example, they show that nonlinear effects are significant for wave amplitudes as low as 3 mγ for a 5-kHz signal at $L = 4$. We provide a quantitative criterion for determining the applicability of the simple linear theory for a given problem. The full distribution computations show that significant precipitated fluxes ($\sim 10^{-1}$ erg/cm^2 s) can be produced with moderate strength waves (10 mγ). These fluxes are within the resolution of the particle detectors designed for the ISEE (International Sun Earth Explorer) satellite program. Our results may therefore also serve as theoretical predictions for that as well as other future experiments.

2. Description of the Physics

Equations of Motion

We consider a circularly polarized monochromatic whistler mode signal of constant amplitude propagating along the static magnetic field $\mathbf{B}_0$. Since the magnetospheric medium is slowly varying, i.e., the variations of medium parameters within the space of one wavelength are negligible, WKB approximation can be used, and the wave magnetic field can be expressed as

$$\mathbf{B}_w = B_w \left[\mathbf{a}_x \cos \left(\omega t - \int_0^z k \, dz \right) + \mathbf{a}_y \sin \left(\omega t - \int_0^z k \, dz \right) \right]$$

where z is the coordinate along $\mathbf{B}_0$, ω is the angular frequency, k is the wave number, and $\mathbf{a}_x$ and $\mathbf{a}_y$ are the unit vectors in the x and y directions, respectively. For whistler mode propagation, which is governed by the thermal (cold) component of the plasma, k is given approximately by

$$k = \frac{\omega_P}{c} \left(\frac{\omega}{\omega_H - \omega} \right)^{1/2}$$

where c is the speed of light, ω_P is the electron plasma frequency, and ω_H is the electron gyrofrequency. In this expression it has been assumed that $(\omega_P/\omega_H)^2 \gg 1$.

Strictly speaking, when a WKB approximation is used to express the wave fields in a slowly varying medium, the wave intensity must also be a function of z. In the magnetosphere, B_w is proportional to $(\omega_H k)^{1/2}$. For the parameter values used in this paper (see Table 1) the important wave-particle interaction occurs within $\pm 20°$ of the equator. Since the wave intensity variation in that range is less than a few percent, we have used a constant B_w in our computations.

We now consider the cyclotron resonance interaction between such a wave and energetic electrons trapped in the flux tube surrounding the field line. Cumulative energy exchange between the waves and electrons will occur only when the Doppler shifted wave frequency is approximately equal to the electron gyrofrequency, i.e.,

$$\omega + k v_{\parallel} \simeq \omega_H \tag{1}$$

where $v_{\parallel}$ and k have the directions shown in Figure 1. Since ω_H must exceed ω in the whistler mode, (1) can be satisfied when the resonant electrons and the wave travel in opposite directions. In the absence of the wave the particles are adiabatically trapped in the earth's magnetic field, and their motion, neglecting the small longitudinal drift, is described by the relations

TABLE 1. Parameter Values for the Example Case

Parameter	Value
Field line	$L = 4$
Equatorial gyrofrequency	$f_{Heq} = 13.65$ kHz
Equatorial cold plasma density	$n_{eq} = 400$ el/cc
Wave frequency	$f = 5$ kHz
Equatorial parallel resonance velocity	$v_R = 1.899 \times 10^7$ m/s
Equatorial parallel resonant energy	$E \simeq 1$ keV
Refractive index at the equator	$n \simeq 40$
Wavelength at the equator	$\lambda_w \simeq 2.2$ km
Trapping period	$t_T = 2\pi[k(eB_w/m)v_\perp]^{-1/2} \simeq 8$ ms for $B_w = 10$ mγ, $\alpha = 30°$, $v_\parallel = v_{\parallel R}$
Trapping length	$l_T \simeq t_T v_{\parallel R} \simeq 150$ km for $B_w = $ mγ, $\alpha = 30°$

$$\dot{v}_\parallel = -\frac{v_\perp^2}{2B_0}\frac{\partial B_0}{\partial z}$$
$$\dot{v}_\perp = +\frac{v_\perp v_\parallel}{2B_0}\frac{\partial B_0}{\partial z} \qquad (2)$$

where the coordinate system and the variables are defined in Figure 1. The effect of the wave on the particle motion is given by the Lorentz force equation

$$\left(\frac{d\mathbf{v}}{dt}\right)_{\text{wave}} = -\frac{e}{m}[\mathbf{E}_w + \mathbf{v}\times\mathbf{B}_w] \qquad (3)$$

where $\mathbf{v} = \mathbf{v}_\perp + \mathbf{v}_\parallel$ is the total velocity of the particle. Writing (3) in a more convenient form and also superimposing the adiabatic motion of the particles as given by (2), we obtain the complete equations of motion for the cyclotron resonance wave-particle interaction:

$$\dot{v}_\parallel = \left(\frac{eB_w}{m}\right)v_\perp \sin\phi - \frac{v_\perp^2}{2\omega_H}\frac{\partial\omega_H}{\partial z} \qquad (4a)$$

$$\dot{v}_\perp = -\left(\frac{eB_w}{m}\right)\left(v_\parallel + \frac{\omega}{k}\right)\sin\phi + \frac{v_\perp v_\parallel}{2\omega_H}\frac{\partial\omega_H}{\partial z} \qquad (4b)$$

$$\dot{\phi} = \omega_H - \omega - kv_\parallel - \left(\frac{eB_w}{m}\right)\left(v_\parallel + \frac{\omega}{k}\right)\frac{\cos\phi}{v_\perp} \qquad (4c)$$

In the above, the angle ϕ is the complement of the angle between the electron's perpendicular velocity ($\mathbf{v}_\perp$) and $\mathbf{B}_w$. Since the medium is inhomogeneous, the quantities ω_H and k are functions of z, the distance along the field line. Equations (4) are written in the laboratory frame, with the coordinate system as described in Figure 1. For our purposes, no important simplification results by transforming to either the wave or the particle frame.

Equations (4) in whole or in part have been used to study VLF wave particle interactions by many authors [*Bell*, 1964, 1965; *Brice*, 1964; *Helliwell*, 1967, 1970; *Dysthe*, 1971; *Nunn*, 1971, 1974; *Palmadesso and Schmidt*, 1971, 1972; *Matsumoto*, 1972; *Ashour-Abdalla*, 1972; *Bud'ko et al.*, 1972; *Crystal*, 1975; *Helliwell and Crystal*, 1973; *Roux and Pellat*, 1976; *Karpman et al.*, 1974*a*, *b*]. *Dysthe* [1971] was the first to include the adiabatic terms in (4*a*) and (4*b*).

The first terms of (4*a*) and (4*b*) are due to the wave-induced longitudinal and transverse forces $\mathbf{v}_\perp \times \mathbf{B}_w$ and $(\mathbf{v}_\parallel \times \mathbf{B}_w + \mathbf{E}_w)$, respectively. The additional terms give the adiabatic variations of $v_\parallel$ and $v_\perp$ that are superimposed on the wave perturbations. It should be noted that although the presence of field-aligned wave forces violates the assumptions underlying the first adiabatic invariant [*Roederer*, 1970], the changes in $v_\parallel$ and $v_\perp$ due to changing static magnetic field intensity can still be described by the differential adiabatic theory at each point during the interaction.

Since the wave terms in (4*a*) and (4*b*) are proportional to sin ϕ, it is apparent that the interaction is strongly controlled by the third equation (4*c*) which gives the variation of ϕ. Cumulative changes in $v_\parallel$ and $v_\perp$ will only result when $\dot{\phi}$ (and $\ddot{\phi}$) is small. The wave term in (4*c*) (last term on the right-hand side) gives the phase change due to the centripetal acceleration of the particle resulting from $(\mathbf{v}_\parallel \times \mathbf{B}_w + \mathbf{E}_w)$ force. We have found that for most magnetospheric parameters the effect of this term is negligible, especially for large pitch angles and/or small wave amplitudes. However, even for wave amplitudes as small as 1 mγ this wave term becomes dominant as soon as the pitch angle falls below 1° or 2°. Note that individual particles that have somewhat larger initial pitch angles could still be scattered down to these low pitch angles during the interaction. At that time this term must be present in the equations in order to describe the correct physics.

In all our computations we have used the complete equations (4). We comment on the role of different terms as we discuss the results.

Total Scattering and the Role of $\partial\omega_H/\partial z$

The equations (4) define the motion of each individual electron. For a particle with initial velocities of $v_{\parallel 0}$ and $v_{\perp 0}$ and an

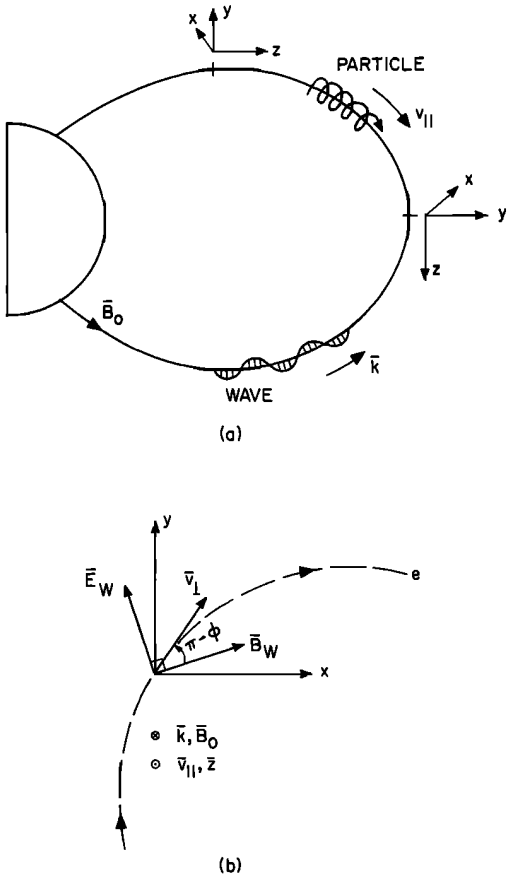

Fig. 1. Coordinate system for the equations of motion. The z axis is everywhere aligned with the magnetic field line. Shown in dashed lines is the orbit of the electron in the x-y plane.

initial phase of ϕ_0, these equations, when properly integrated over time, give the resulting $\Delta v_\parallel$ and $\Delta v_\perp$ for that particle. In other words,

$$\Delta v_{\parallel,\perp} = \int_0^{T_I} \dot{v}_{\parallel,\perp}\, dt \tag{5}$$

where T_I is the interaction time. In principle, the integration must be carried out for $T_I \to \infty$. However, because of the changing ω_H due to the inhomogeneity of the field the resonance condition (1) can be satisfied only over a limited region along the field line for any given particle. When (1) is not satisfied, it is apparent from (4*c*) that $|\dot{\phi}|$ would be large and the wave contributions to $\dot{v}_\parallel$ and $\dot{v}_\perp$ will be noncumulative. Therefore a time T_I can be defined over which the wave-induced perturbations are significant.

The wave-induced changes $\Delta v_\parallel$ and $\Delta v_\perp$ and the corresponding pitch angle change $\Delta\alpha$ are hereafter referred to as scattering. As is apparent from (4), the point-to-point scatterings (and therefore the integrated total scatterings) are dependent on the initial values of $v_\parallel$ and $v_\perp$, as well as on the initial phase ϕ_0 between $v_\perp$ and $-B_w$ at the time of encounter between the wave and the particle. The scattering is also dependent on wave parameters B_w, ω, and k and medium parameters ω_H and $\partial\omega_H/\partial z$. In general, when the resonance occurs away from the equator, the cumulative interaction time is shortened (since $\partial\omega_H/\partial z$ is larger), and the total scattering is smaller. The quantity $\partial\omega_H/\partial z$ is the principal factor in determining the interaction time T_I.

In order to see the effect of $\partial\omega_H/\partial z$ clearly, we follow a procedure similar to that used by *Dysthe* [1971]. Taking the time derivative of both sides of (4*c*) and neglecting the wave terms on the right-hand side, we can make use of (4*a*) to rewrite (4*c*) as [*Inan*, 1977]

$$\ddot{\phi} + k\left(\frac{eB_w}{m}\right) v_\perp \sin\phi = \left[\frac{3}{2} + \frac{\omega_H - \omega}{2\omega_H}\tan^2\alpha\right] v_\parallel \frac{\partial\omega_H}{\partial z} \tag{6}$$

In deriving (6) we have made use of the fact that in a diffusive equilibrium model of the cold plasma, such as the one used in this paper, the plasma frequency ω_P is approximately constant along the field line and that for resonant particles $v_\parallel \simeq (\omega_H - \omega)/k$. Equation (6) is a type of 'pendulum' equation which gives the variation of the phase ϕ. The forcing function of this equation is proportional to $\partial\omega_H/\partial z$, hence demonstrating the influence of the term $\partial\omega_H/\partial z$, i.e., the inhomogeneity force, in controlling the interaction. The total interaction time T_I is determined by the relative magnitudes of this forcing function and the restoring 'force' (the wave force) of the pendulum, which is proportional to $k(eB_w/m)v_\perp$. When $B_w = 0$, it can be shown that (6) is equivalent to (15) of *Helliwell* [1970] when $N = 0$ and $A = 0$ in the latter equation.

Method of Solution

Since the equations of motion are highly nonlinear, it is difficult to evaluate the integrals in (5) by using analytical methods unless one makes restrictive simplifying assumptions. One common approach is to use linear theory [*Das*, 1971; *Ashour-Abdalla*, 1972]. According to this theory, the perturbations in $v_\parallel$ and $v_\perp$ are computed by using field components at the position of the particle as given by the unperturbed ($B_w = 0$) motion. In effect, the unperturbed phase variation obtained from (4*c*) with $v_\parallel$ varying only because of adiabatic forces is substituted into (4*a*) and (4*b*), and the perturbations $\Delta v_\parallel$ and $\Delta v_\perp$ are computed. Although it is generally agreed that linear theory is applicable for sufficiently low wave amplitudes, none of the authors who have employed this theory in their analyses have given quantitative criteria to justify their assumptions.

Our approach to the solution of equations (4) is to use a test particle simulation of the wave-particle interaction. The idea is that the perturbation of the full particle distribution can be inferred by considering the effect of the wave on a sufficient number of test particles that are appropriately distributed in ϕ, $v_\parallel$, and $v_\perp$. With this point of view, the problem is one of classical Newtonian mechanics. Namely, given a wave structure, the task is to simulate the equations of motion for individual test particles. In the next section we describe the computer simulation in some detail. With the simulation approach it is possible to use the full equations of motion and to test quantitatively the relative importance of different terms. Section 4 gives a detailed quantitative study of the interaction using single-particle trajectories and compares the results of our full nonlinear analysis with those obtained by using linear theory. As a practical application of the computer simulation, in section 5 we calculate the precipitated flux for a particular case. Although the precipitated flux is the important measurable quantity, the study of single-particle trajectories is important for bringing out the physics of the interaction. Once the physical behavior and the methods of calculation are established, the full distribution calculations for different cases then become straightforward computer experiments.

3. Description of the Simulation

The computer simulation employs a centered dipole model for the static magnetic field and a diffusive equilibrium model for the cold plasma density. The necessary input to this portion of the program consists of wave frequency, L value, and equatorial cold plasma density n_{eq}. The parameters of the medium, i.e., $\omega_H(z)$ and $k(z)$, are then computed over the length of the field line to which that particular calculation is limited. These values are stored for later use in the simulation.

In a test particle simulation each particle must be identified with a set of unique and constant parameters. For adiabatically trapped particles the equatorial pitch angle α_{eq} and equatorial parallel velocity $v_{\parallel eq}$ are one such set of quantities. By using the first adiabatic invariant the local pitch angle α and parallel velocity $v_\parallel$ at any other point z can be readily obtained from α_{eq} and $v_{\parallel eq}$:

$$\sin\alpha = \sin\alpha_{eq}(B(z)/B_{eq})^{1/2} \tag{7a}$$

$$v_\parallel = (B(z)/B_{eq})^{1/2} v_{\parallel eq} \tan\alpha_{eq}/\tan\alpha \tag{7b}$$

where B_{eq} and $B(z)$ represent the equatorial and local values of the static magnetic field, respectively.

In the absence of the wave a test particle described by α_{eq_0} and $v_{\parallel eq_0}$ will acquire the local pitch angle and parallel velocity as given by (7*a*) and (7*b*) as it moves along the field line. Significant cumulative interaction between the wave and the particle will occur only in the vicinity of the point where $v_\parallel \simeq v_R$, v_R being the local resonant velocity, given by $v_R = (\omega_H - \omega)/k$. As indicated in Figure 2, this condition will be satisfied in the vicinity of two locations along the field line, owing to the symmetry of the dipole field. Since the wave-induced perturbations will be negligible outside these regions, the particle motion at locations other than these can still be described by (7*a*) and (7*b*). The encounter with the wave modifies the local $v_\parallel$ and α and, through (7*a*) and (7*b*), the equatorial parameters α_{eq} and $v_{\parallel eq}$ to be associated with that particle.

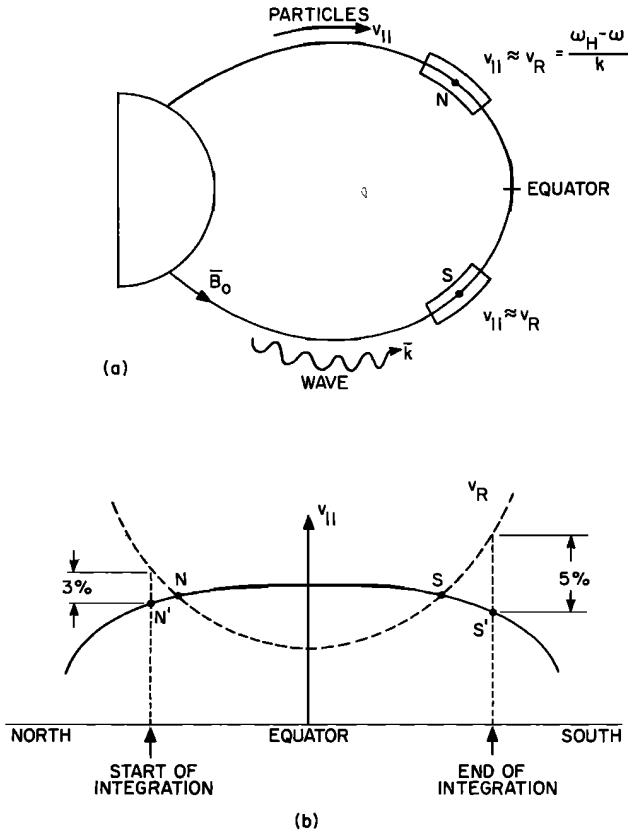

Fig. 2. Complete interaction of the wave and a test particle: (*a*) In general, the cyclotron resonance condition (1) will be satisfied at two locations N and S along the field line. (*b*) Adiabatic variation of the particle parallel velocity with distance from the equator. Shown in dashed lines is the resonance velocity v_R. The integration of the equations of motion starts at point N' and ends at S' for the simulation of the complete interaction.

For a monochromatic CW signal traveling from south to north that has a constant intensity over the whole field line, the complete interaction of each particle with the wave will involve the following: As the particle approaches its point of resonance in the northern hemisphere, the wave-induced perturbations become increasingly significant. When the particle moves past its resonance point, having been scattered in α_{eq} and $v_{\parallel eq}$, the perturbations decrease until it reaches the equator. Past the equator, the particle approaches its second resonance point and is scattered again. Depending on the distance between the two resonance points, the two encounters may or may not be in phase with each other.

To simulate this complete interaction, the equations of motion must be integrated from the time the particle is close enough (usually within 2–3% in $v_{\parallel}$) to its first resonance point to experience significant perturbations to the time at which the particle has passed significantly beyond its second resonance point so that the wave perturbations become negligible.

Figure 2*b* shows the adiabatic variation of the particle parallel velocity along the field line. Shown in dashed lines is the local resonance velocity v_R. The input to the main simulation part of the program is a set of values α_{eq_0}, $v_{\parallel eq_0}$ and an initial phase ϕ_0. With these parameters specified, the program transfers α_{eq} and $v_{\parallel eq}$ into local values α and $v_{\parallel}$ using (7*a*) and (7*b*), going progressively away from the equator, and at each point checking $|v_{\parallel} - v_R|$ in order to locate the vicinity of the resonance point N. The integration is started at a point where $v_{\parallel}$ is within some percentage of the resonance velocity of the northern resonance point. We have found that when the particle is more than ~3% away from local resonance, the wave-induced perturbations are not significant. This value is used in our computations as indicated in Figure 2*b*. The integration is carried out until the time where $\epsilon = |(v_{\parallel} - v_R)/v_R| > 0.05$ and $d\phi > 2\pi$. Both these criteria are very conservative and were established by examining single-particle trajectories. If the complete interaction is to be simulated, the integration is carried out until the particle passes its resonance point S in the southern hemisphere even if ϵ gets to be greater than 0.05 in between its first and second resonances.

At the end of the integration the local pitch angle α_F (F for final) and parallel velocity $v_{\parallel F}$ at the point where the integration is stopped are found. These values are then transformed through (7*a*) and (7*b*) to equatorial values α_{eq_F} and $v_{\parallel eq_F}$ for that particle. The difference $\alpha_{eq_F} - \alpha_{eq_0} = \Delta\alpha_{eq}$ gives the total pitch angle scattering suffered by the particle.

For a monochromatic CW signal that is generated or strongly amplified in a narrow region around the equator, as predicted by VLF emission generation theories [*Helliwell*, 1967, 1970; *Nunn*, 1974], the wave intensity can be assumed to be constant on the northern side of the equator and zero on the southern side. The complete interaction in that case involves only one scattering in the vicinity of the resonance point N.

In addition to simulating the complete interaction of each test particle with the wave, as is necessary for the full distribution computations, the computer code can also be used for studies of different portions of the interaction. This is done in the next section where we study the scattering of particles that are initially resonant with the wave at the equator.

4. Study of the Interaction

Scattering of a Single Resonant Sheet

Our purpose in this section is to give a clear presentation of the different aspects of the physics of the interaction.

Although the full distribution calculations give useful measurable quantities, such as the precipitated flux, they are not very helpful in understanding the physics of the interaction. The behavior of single particles provides much better insight, illustrating the effect of various parameters such as B_w, α_{eq}, n_{eq}, L, and initial phase ϕ_0. We study the case of initially resonant electrons, uniformly distributed in ϕ and moving away from the equator. The interaction starts at the equator for most cases. The use of initially resonant particles enables us to present clearly the initial phase dependence. The equator is chosen because the inhomogeneity there is a minimum, thus enabling us to see the full effect of the wave forces. We must emphasize at this point that this choice is made only to simplify the presentation and does not affect the physics. In a distribution of particles interacting with a wave at any instant of time, there will be particles with many values of α_{eq} and $v_{\parallel eq}$ located at all points along the field line. In this section we consider a sheet of electrons that meets the wave at the equator with specified α_{eq} and $v_{\parallel eq}$ values. The results are qualitatively representative of those for most other sheets in the distribution, although the amount of scattering will in general be smaller for interactions away from the equator or for nonresonant sheets.

The parameter values used for most of our calculations are given in Table 1; they represent a realistic magnetospheric case. $L = 4$ is chosen because it is close to the location of the VLF transmitter at Siple, Antarctica, from which many of the

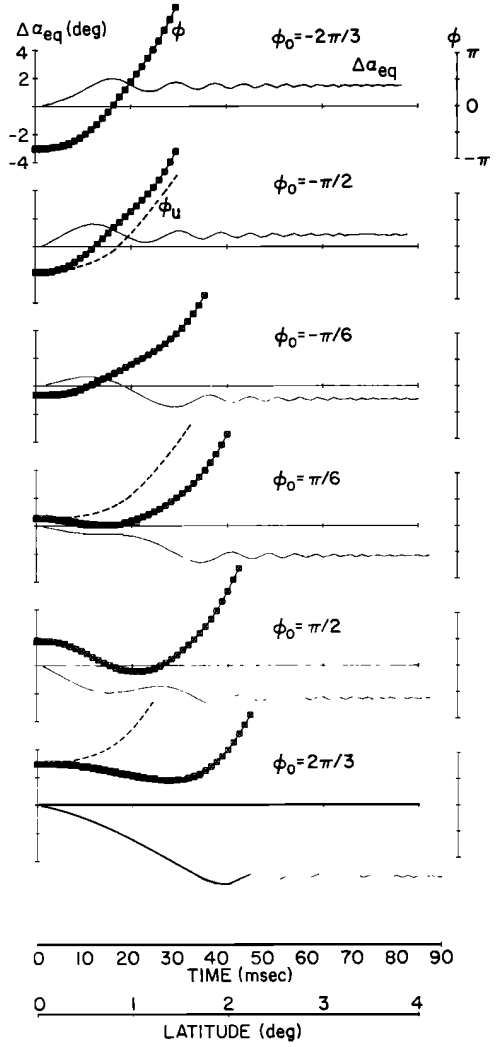

Fig. 3. Single-particle trajectories for $B_w = 10$ mγ. Both the total scattering $\Delta\alpha_{eq}$ (solid lines) and the phase ϕ (squared points) are shown as functions of time. All particles start at resonance at the equator (see Figure 4, top panel) and move southward into the wave. Particle trajectories for six different initial phases are shown. The phases are chosen to illustrate typical trajectories The dashed lines are the unperturbed phase (ϕ_u) variation for the case of $B_w = 0$. For all trajectories, $\alpha_{eq} = 10°$.

experimental data have come. A wave frequency of 5 kHz is chosen, a frequency often used in the Siple wave injection experiments.

We first consider particles with an equatorial pitch angle $\alpha_{eq_0} = 10°$ and a wave amplitude of $B_w = 10$ mγ. Figure 3 shows the computed trajectories for six particles distributed in initial phase ϕ_0. We have plotted both $\Delta\alpha_{eq}$ and phase ϕ at each step of the interaction. The resonant interaction starts at the equator for all particles.

Consider, for example, the particle with $\phi_0 = -2\pi/3$. As this particle moves away from the equator, it suffers a positive $\Delta\alpha_{eq}$, and as $\dot{\phi}$ increases (the particle gyrating faster with respect to the wave), the changes in $\Delta\alpha_{eq}$ become smaller and smaller. Eventually, the oscillations become insignificant, and the particle leaves the interaction region with a net change in equatorial pitch angle. Note that α_{eq} of each of the six particles in Figure 3 can be considered unaffected by the wave after about 70 ms (3° latitude). Beyond this point the wave-induced particle scatterings are not cumulative.

Also shown in Figure 3 is the unperturbed phase $\phi_u(t)$ (i.e., the phase variation for negligible wave intensity) for some initial phases. The $\phi_u(t)$ variation for other phases is exactly the same in form but shifted up or down depending on ϕ_0.

For particles starting at resonance (i.e., $v_\parallel$ satisfies (1)), $\dot{\phi}_0 \simeq 0$. For $B_w \simeq 0$, as the particle moves away from the equator ω_H increases, therefore increasing $\dot{\phi}$, which causes ϕ to increase, as

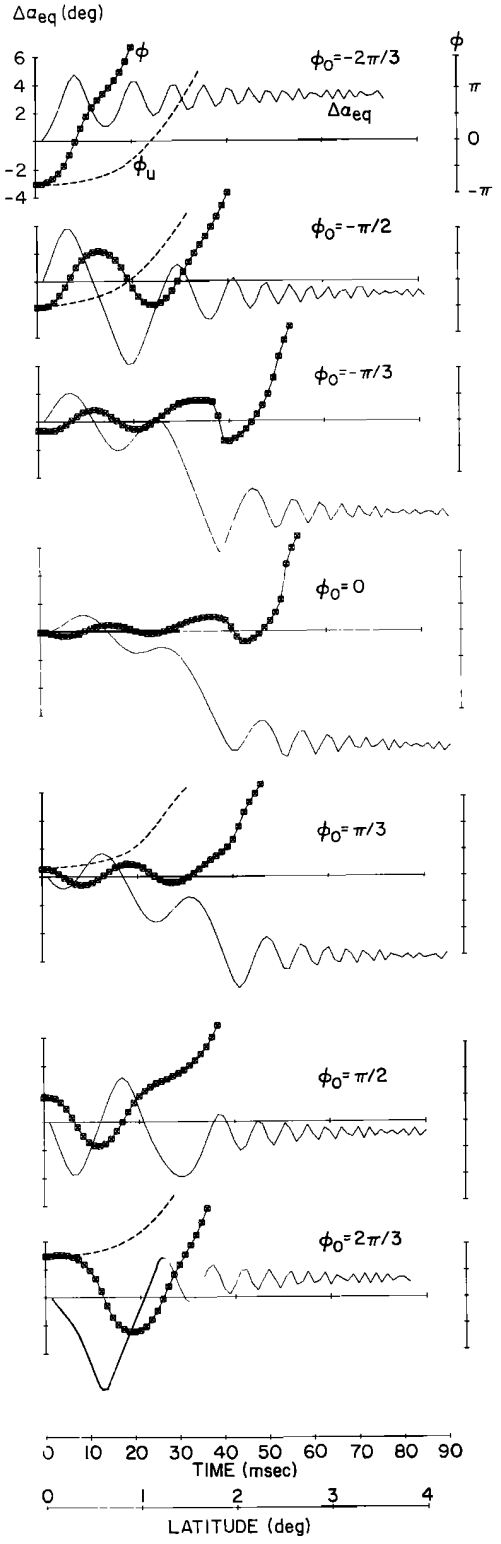

Fig. 4. Single-particle trajectories for $B_w = 50$ mγ. The format is the same as Figure 3. For all trajectories, $\alpha_{eq_0} = 10°$.

can be seen from the ϕ_u variation in Figure 3. In other words, $\ddot{\phi}_0 = \ddot{\phi}_u > 0$. For $B_w \neq 0$, the interaction can be studied qualitatively as follows.

1. For negative ϕ_0, $\dot{v}_{\parallel 0} < 0$. (See equations (4*a*).) Hence $v_\parallel$ decreases while ω_H increases as the particles move away from the equator. Therefore $\ddot{\phi}_0 > \ddot{\phi}_u$, and the time for which the particle stays within resonance is shortened. Also, since the initial wave-induced $\dot{v}_\parallel$ is negative, the local pitch angle of the particle increases, which in turn through (7*a*) transforms into an increase in the equatorial pitch angle. As ϕ increases to the point where sin ϕ changes sign (in this case becomes positive), $\dot{v}_\parallel$ becomes positive and tends to decrease ϕ. Since ω_H keeps increasing, the wave forces offset the effects of the inhomogeneity at this stage of the interaction. However, there already is a large $\dot{\phi}$, and the particle is no longer near resonance. Therefore if the wave amplitude is not strong enough to cause an oscillation (or reversal) in phase (i.e., trapping), the phase angle ϕ continues to increase. When ϕ comes to the point where sin ϕ again changes sign, $\dot{v}_\parallel$ again becomes negative. The periodic changes of sign of $\dot{v}_\parallel$ lead to oscillations in $\Delta\alpha_{eq}$. This behavior is most clearly illustrated by the case of larger wave amplitudes, as in Figure 4. Since ω_H continuously increases as the particle moves away from the equator, the period of these oscillations decreases as the particle moves away from resonance. Eventually, the particle acquires a net pitch angle change $\Delta\alpha_{eq}$. Typical trajectories for the negative initial phase case are shown in Figure 3.

2. For positive ϕ_0, $\dot{v}_{\parallel 0} > 0$, and the wave forces offset the effects of the inhomogeneity. Therefore $\ddot{\phi} < \ddot{\phi}_u$, and the time during which the particle stays within resonance is increased, hence allowing more scattering due to more exposure to cumulative interaction. For the case of $B_w = 10$ mγ, given in Figure 3, we see that final scatterings for $\phi_0 > 0$ are generally larger than those for $\phi_0 < 0$, although the final scattering depends, as we shall later see, on a wide variety of parameters. Note in Figure 3 that although the initial $\dot{v}_\parallel$ is a maximum for $\phi_0 = \pi/2$, the final scattering is the largest for $\phi_0 = 2\pi/3$. This occurs because for $\phi_0 = 2\pi/3$ the wave and inhomogeneity forces balance each other over a longer distance and hence $\ddot{\phi}$ stays very close to zero, therefore increasing the time spent within resonance.

For an initial pitch angle of 10° a wave amplitude of 10 mγ is not large enough to cause more than one oscillation in phase ϕ. In Figure 4 we give the trajectories of seven particles for $B_w = 50$ mγ. In comparing Figures 3 and 4 we make the following observations:

1. The oscillations in $\Delta\alpha_{eq}$ as the particle moves away from resonance are larger in amplitude for $B_w = 50$ mγ than for $B_w = 10$ mγ. This is expected, since the scattering at each point is proportional to B_w.

2. For some of the phases ($\phi_0 = -\pi/2, -\pi/3, 0, \pi/3$) the particle phase $\phi(t)$ makes more than one oscillation. Hence the particle is phase trapped, although only for a short while. Trapping is maximum for $\phi_0 = 0$.

3. All the trapped particles end up with a negative $\Delta\alpha_{eq}$. This is because for trapped particles $v_\parallel \simeq v_R = (\omega_H - \omega)/k$ and $\dot{v}_\parallel \simeq \dot{v}_R$. Since $\dot{v}_R > 0$ when moving southward from the equator, $\dot{v}_\parallel > 0$ and, from (4*b*), $\dot{v}_\parallel < 0$. Thus the pitch angle must decrease for all trapped particles as they move away from the equator.

4. Consider the trajectory for the $\phi_0 = -\pi/3$ particle. The second minimum of $\Delta\alpha_{eq}$ (at $t \simeq 40$ ms) seems much sharper than for other cases. Note that the particles shown in Figure 4 have an equatorial pitch angle of $\alpha_{eq} = 10°$. The second minimum in $\Delta\alpha_{eq}$ for $\phi_0 = -\pi/3$ is at about $\Delta\alpha_{eq} = 9.5°$. In other words, as the pitch angle continuously decreases, it has reached a point where it is very close to zero. At those low pitch angles, $v_\perp$ is very small, and therefore the wave term ($\propto \cos\phi/v_\perp$) in (4*c*) becomes significant, causing a large change in phase which prevents the pitch angle from reaching zero. This effect has been called the 'loss cone reflection' effect [*Inan*, 1977]. This example shows the importance of not deleting this term in the computations. Without this term the pitch angle would have gone negative. At the third minimum of $\Delta\alpha_{eq}$ for $\phi_0 = 0$ we have the same effect, again clearly seen by an abrupt change in ϕ.

Note that the particles shown in Figures 3 and 4 have gone through significant net pitch angle scatterings ranging from a few percent to almost 100% of their initial pitch angle. It is important to point out that the energy scattering of all of these particles is less than a few percent. This is because the wave magnetic field forces are the controlling forces in the cyclotron resonance interaction in the magnetosphere. These forces change the direction of momentum of the particle (pitch) and

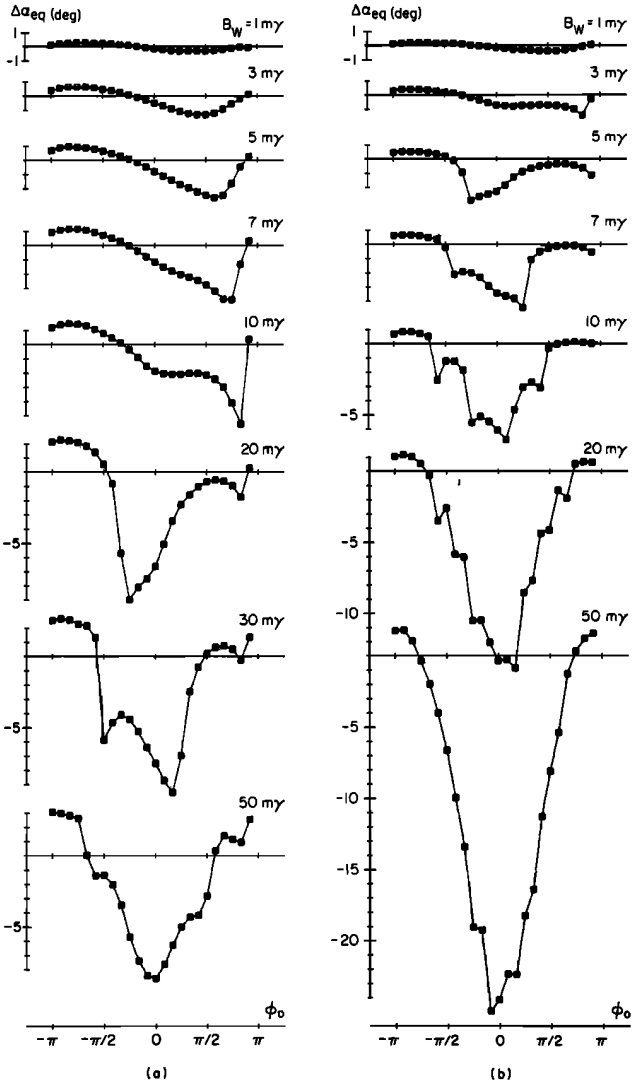

Fig. 5. Total scattering $\Delta\alpha_{eq}$ versus initial phase for different wave amplitudes for $L = 4$ and $n_{eq} = 400$ el/cc: (*a*) $\alpha_{eq} = 10°$ and (*b*) $\alpha_{eq} = 30°$. Each square in the figures shows the scattering of an individual test particle. Twenty-four particles, uniformly distributed in ϕ_0, are used in each sheet.

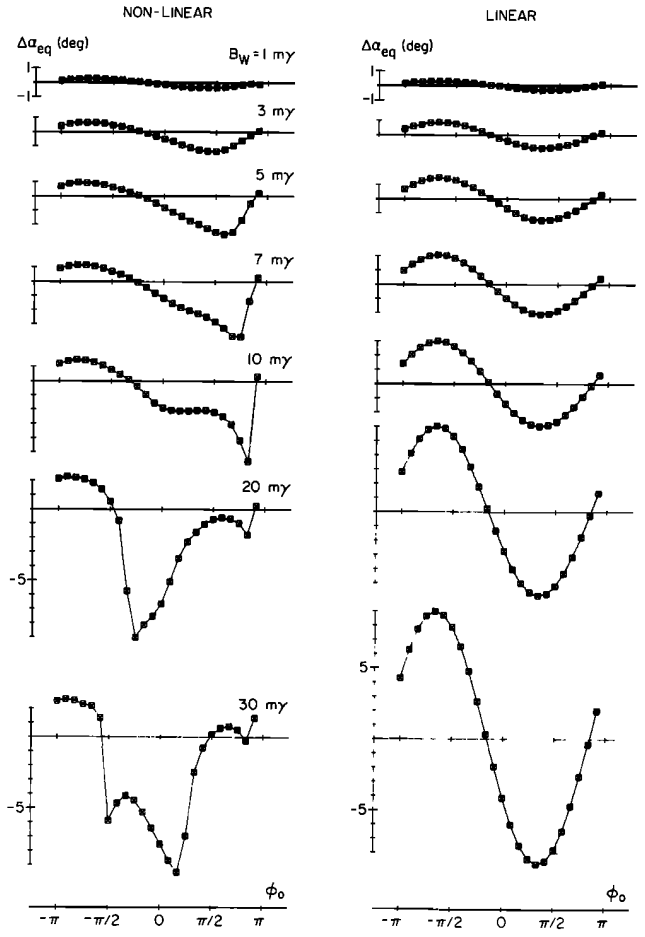

Fig. 6. Comparison of results of linear theory and the full nonlinear analysis. The total scattering versus ϕ_0 is given for $\alpha_{eq} = 10°$ and for different wave amplitudes. The format is similar to that of Figure 5.

not its energy. Some energy exchange occurs through the electric field of the wave.

After the preceding discussion of the single-particle trajectories it is enlightening to study the collective motions of particles uniformly distributed in phase. As our tool for this study we consider the variation of the final scattering $\Delta\alpha_{eq}$ versus initial phase. We have found that the nature of the interaction and the effects of different parameters are most clearly presented in such a format. Below, we give results of our computations for 24 electrons equally distributed in initial phase ϕ_0. We consider different cases to isolate the effects of parameters such as B_w, α_{eq}, n_{eq}, position of resonance, etc. The results are obtained by integrating the full equations of motion for each of the 24 electrons in the sheet to obtain the total final scattering $\Delta\alpha_{eq}$. We then plot $\Delta\alpha_{eq}$ versus initial phase ϕ_0 and discuss each result qualitatively.

Effects of the wave amplitude. Figure 5*a* shows $\Delta\alpha_{eq}$ versus ϕ_0 for the parameters as given in Table 1 and for $\alpha_{eq_0} = 10°$. We have given results for a range of wave amplitudes from $B_w = 1$ mγ to $B_w = 50$ mγ. For low wave amplitudes such as $B_w = 1$ mγ and 3 mγ we have 'linear' scattering. In other words, for these cases the inhomogeneity is the dominant factor in controlling $\phi(t)$ rather than the wave forces. Therefore $\phi(t) \simeq \phi_u(t)$, and linear theory can be applied. It can be shown that the shape of the $\Delta\alpha_{eq}$ versus ϕ_0 curves is approximately sinusoidal for these cases [*Inan*, 1977]. In the rest of this paper the interaction will be termed to be in the linear mode whenever $\Delta\alpha_{eq}$ versus ϕ_0 is approximately sinusoidal.

For $B_w > 7$ mγ the curves change shape. For $B_w = 50$ mγ we have what we call the 'trapped' mode. The trapped mode is one in which the wave forces play the dominant role in controlling $\ddot{\phi}$. The phase ϕ in this case goes through more than one oscillation due to sign changes of $\ddot{\phi}$. As was discussed above in connection with Figure 4, the trapped particles end up with a net negative change in pitch angle, thus producing a $\Delta\alpha_{eq}$ versus ϕ_0 variation as shown in Figure 5*a* for the $B_w = 50$ mγ case. Note that only particles in a range around $\phi_0 = 0$ are trapped; the initial phases of other particles are not appropriate for trapping. This is also seen in Figure 4.

Figure 5 gives only the final net scatterings. No time parameter is involved. For each case, the equations have been integrated for each electron in the sheet until the particle is no longer significantly affected by the wave. The total pitch angle change $\Delta\alpha_{eq}$ is then plotted against ϕ_0. Note that for 7 mγ $< B_w <$ 50 mγ the $\Delta\alpha$ versus ϕ_0 curves resemble neither the linear nor the trapped mode. This is because for these transition values neither the wave force nor the inhomogeneity is clearly dominant. For $B_w = 3$ mγ and 5 mγ we observe from Figure 5*a* that there is an asymmetry between scattering for negative and positive initial phases. This comes about because although for all ϕ_0 the inhomogeneity is the dominant factor, for positive ϕ_0 the wave forces offset the effects of the inhomogeneity, whereas for negative ϕ_0 the wave force adds to the effect of the inhomogeneity. Therefore for positive ϕ_0 the particle stays in resonance for a longer time and hence experiences larger scattering.

For $B_w = 50$ mγ, Figure 5 shows that the maximum negative scattering for $\alpha_{eq_0} = 10°$ is about $\Delta\alpha_{eq} = 9°$. Thus the absolute pitch angle for these particles is reduced nearly to zero. Similarly, for $\alpha_{eq} = 30°$ the maximum negative scattering is 24°, bringing this particle to the edge of the loss cone.

One important point that must be kept in mind is the following: Figure 5*a* shows results for particles traveling away from the equator. Consider the case of particles traveling toward the equator. By studying (4*c*) we see that $\Delta\alpha_{eq}$ versus ϕ_0 variations would be approximately a mirror image of the result for the $B_w = 50$ mγ, with the trapped particles having a net positive pitch angle change. Therefore one should not try to make predictions about the precipitated flux or other full distribution quantities using only these results. The single-particle results given in this section are intended only as an aid to understanding the interaction and sorting out the dependence of $\Delta\alpha_{eq}$ on various parameters.

For higher α_{eq_0} one would expect the deviation from the linear mode to start at lower amplitudes. In Figure 5*b* we show the results for $\alpha_{eq_0} = 30°$ in the same format as Figure 5*a*. We see that the case of $B_w = 3$ mγ is as much away from the linear mode as the case of $B_w = 10$ mγ for $\alpha_{eq_0} = 10°$. This is explained by the fact that the wave-induced $\dot{v}_{\parallel}$ is proportional to $v_\perp B_w$ and therefore to $\tan\alpha_{eq_0}$. As B_w is increased further, we again have a similar kind of transition to the trapped mode. However, the minima of $\Delta\alpha_{eq}$ are much deeper than they are in the $\alpha_{eq_0} = 10°$ case. For $B_w = 50$ mγ, for example, the most stably trapped particle ($\phi_0 = 0$) undergoes a net scattering of almost 24°. The behavior in Figures 3, 4, 5*a*, and 5*b* also clearly shows the difference between coherent and incoherent interactions. In the coherent interaction the particle can be phase locked with the wave and lose almost all of its perpendicular energy in a single encounter with the wave. In contrast, in an incoherent interaction the scatterings suffered

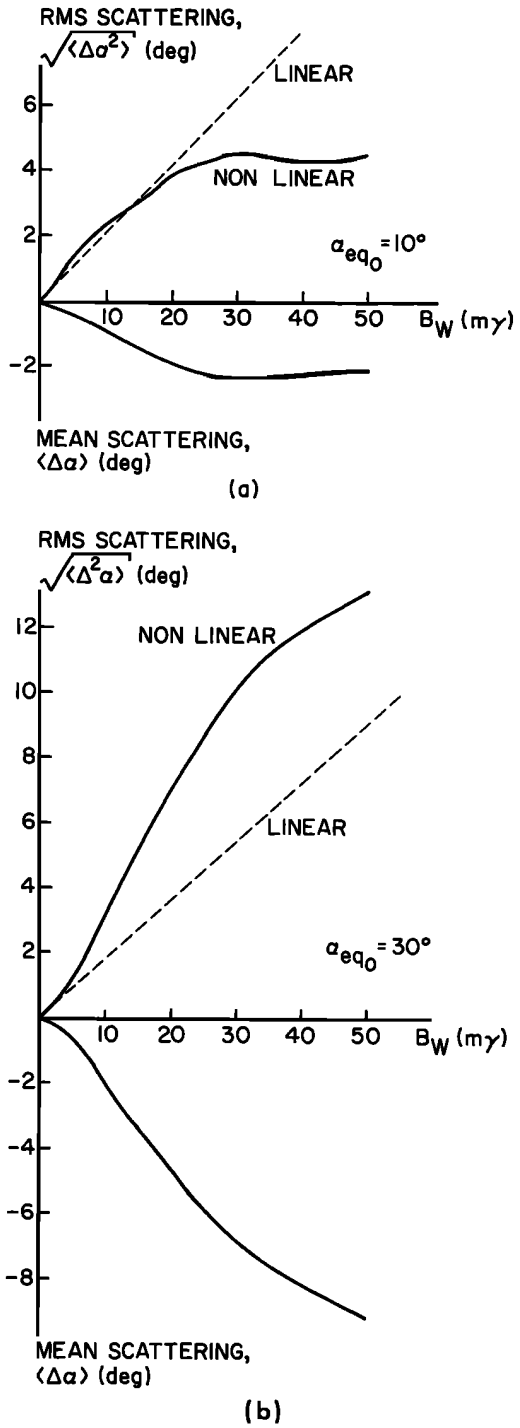

Fig. 7. The rms and mean scattering for linear and nonlinear analyses as a function of wave amplitude. The mean scatterings for the linear case is zero: (*a*) α_{eq_0} = 10° and (*b*) α_{eq_0} = 30°.

by the particle at each instant are random in direction and magnitude. As a result the particles execute a random walk in pitch angle space and a diffusion in the average direction of the field results. Therefore the net total scatterings at each encounter with the wave are generally much smaller.

Comparison with the linear theory. At this point we are ready to compare quantitatively the results of our full analysis with those of linear theory. For purposes of comparison we have arranged our computer program to integrate the motion equations using linear theory if that is desired. Figure 6 shows a comparison of the linear and nonlinear analyses for α_{eq} = 10°. For the linear case the $\Delta\alpha_{eq}$ versus ϕ_0 variation is proportional to $B_w \sin(\phi_0 + \beta)$, where β is a function of initial $v_{\parallel}$ and $v_\perp$ [*Inan*, 1977]. We see from Figure 6 that the difference between the linear and the nonlinear results becomes apparent for $B_w \gtrsim 5$ mγ. Even for B_w = 3 mγ, the asymmetry between the scatterings for positive and negative ϕ_0 is apparent for the nonlinear case. Note that for higher α_{eq_0} the deviation from linear theory occurs at lower wave intensities. For instance, for α_{eq_0} = 30° and B_w = 3 mγ the interaction is clearly nonlinear, as can be seen from Figure 5*b*. Note also that for the linear case the phase variation is the same for all 24 particles in the sheet. Therefore they all spend the same amount of time in resonance.

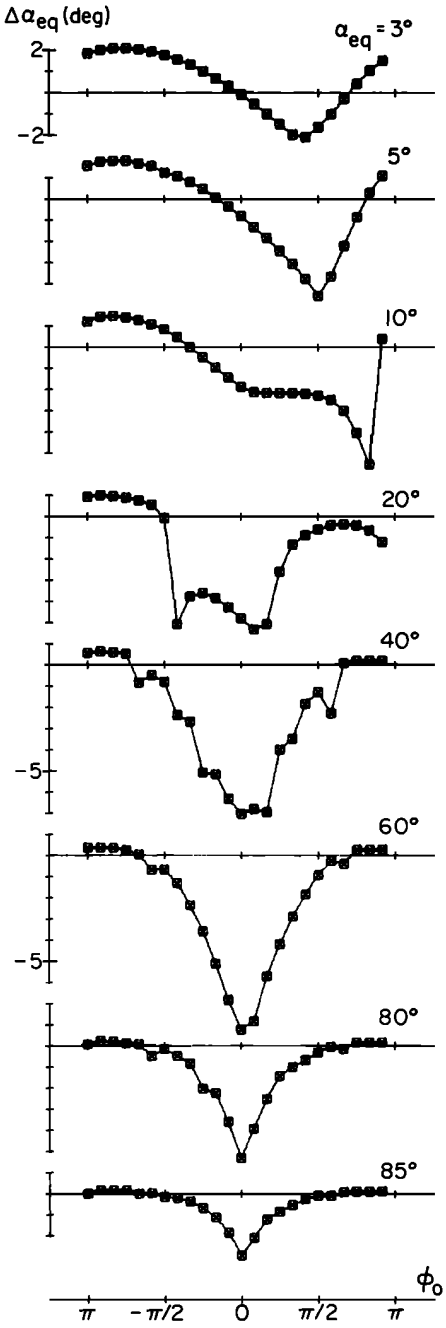

Fig. 8. Initial pitch angle dependence of the total scattering versus ϕ_0 for n_{eq} = 400 el/cc and B_w = 10 mγ. The format is the same as that of Figure 5.

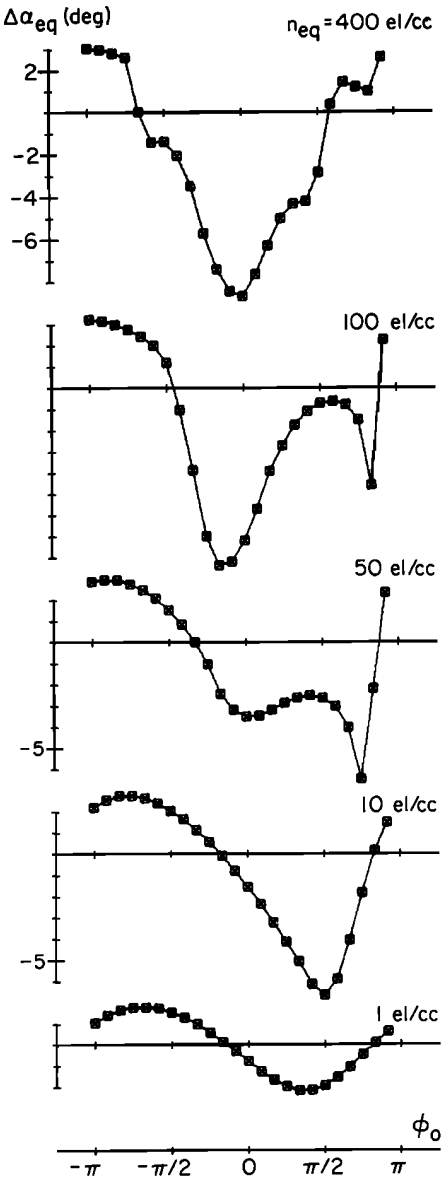

Fig. 9. Variation of total scattering with equatorial cold plasma density n_{eq}. For all cases, $L = 4$, $f = 5$ kHz, $B_w = 50$ mγ, and $\alpha_{eq_0} = 10°$. For $n_{eq} = 1$ el/cc the parallel resonant particle velocity is relativistic. However, the appropriate correction has not been made, since it would only vary the amplitude of the scattering. Our main concern is the shape of the $\Delta\alpha_{eq}$ versus ϕ_0 curves.

Figures 7*a* and 7*b* compare the linear and nonlinear root mean square scattering (i.e., $\langle\Delta\alpha^2\rangle^{1/2}$, where angle brackets denote averaging over the initial phases) and the mean value (i.e., $\langle\Delta\alpha\rangle$) of the $\Delta\alpha_{eq}$ versus ϕ_0 curves for both $\alpha_{eq_0} = 10°$ and 30° cases. We see that for the nonlinear case the mean value increases with wave intensity, whereas for the linear case it is zero for all wave amplitudes. For $\alpha_{eq_0} = 30°$ and for small wave fields of up to 3 mγ the rms scattering for both cases is about the same. However, for higher fields the rms scattering for the nonlinear case deviates from that of the linear case. Therefore the use of linear theory when $B_w > 3$ mγ causes an error in both mean and rms scatterings.

Since for $B_w \geq 40$ mγ, $\Delta\alpha_{eq} \simeq \alpha_{eq_0}$, the rms scattering saturates for the $\alpha_{eq_0} = 10°$ case; however, for the higher initial pitch angle ($\alpha_{eq_0} = 30°$) the rms scattering is considerably larger than the linear result over a wide range of wave amplitudes. The scattering is larger because the nonlinear formulation takes particle trapping into account, and this effect considerably increases the length of the interaction region over which scattering takes place.

Since the $\Delta\alpha_{eq}$ versus ϕ_0 curve for the linear case is found to have a sinusoidal shape, it is possible to readily identify linear or trapped behavior by qualitatively examining the $\Delta\alpha_{eq}$ versus ϕ_0 curves. For example, for the case of Figure 5*a* we see that deviation from a sinusoidal shape starts around $B_w = 5$ mγ and hence linear theory is applicable only for $B_w < 5$ mγ. In the following cases we shall use this concept to study our results.

Dependence on equatorial pitch angle. To isolate the effect of the initial equatorial pitch angle, we hold the wave amplitude constant at $B_w = 10$ mγ and for the parameters of Table 1 compute the scatterings for different α_{eq_0}. Figure 8 shows $\Delta\alpha_{eq}$ versus ϕ_0 curves parameterized in α_{eq_0}. A wide range of pitch angles $3° \leq \alpha_{eq_0} \leq 85°$ is covered. Since the wave-induced $\dot{v}_{\parallel}$ is proportional to $v_\perp$ and hence to tan α_{eq_0}, for sufficiently small pitch angles a linear $\Delta\alpha_{eq}$ versus ϕ_0 variation is expected. Indeed, from Figure 8 we see that the variation for $\alpha_{eq_0} = 3°$ is essentially linear. The deviation from linearity increases as α_{eq_0} is increased, and we have the trapped mode for $\alpha_{eq_0} \gtrsim 30°$. The transition from the linear to the trapped mode is similar to that shown in Figure 5*a*.

For $\alpha_{eq_0} > 60°$, the minimum of the $\Delta\alpha_{eq}$ versus ϕ_0 curves starts to contract. Although the shape of $\Delta\alpha_{eq}$ versus ϕ_0 corresponds to the trapped mode, the total scattering for each particle continuously decreases. The reason for this is that for these high values of α_{eq_0} the variation in the particles' $v_{\parallel}$ and $v_\perp$ due to the adiabatic mirror force (second terms on the right-hand side in (4*a*) and (4*b*)) becomes more and more rapid. Therefore the resonance time and hence the scattering are both reduced.

Dependence on the equatorial cold plasma density. One other parameter which defines the properties of the medium and the wave is n_{eq}, the equatorial cold plasma density. The wave number k is proportional to $n_{eq}^{1/2}$. In Figure 9 we give results for a $B_w = 50$ mγ wave and $\alpha_{eq_0} = 10°$ particles at $L = 4$. We show $\Delta\alpha_{eq}$ versus ϕ_0 curves for different n_{eq} values, ranging from 400 el/cc (inside the plasmapause) to 1 el/cc (outside the plasmapause).

Figure 9 shows that for $n_{eq} = 400$ el/cc a trapped mode exists. Decreasing n_{eq} results in a transition similar to those seen before, to a linear mode for $n_{eq} = 1$ el/cc. This result shows clearly that interactions outside the plasmapause result in less scattering than those inside the plasmapause. This interesting result can be understood as follows: As n_{eq} decreases, the wave phase velocity increases, and the parallel resonant velocity becomes higher. Higher-energy particles move more quickly through the wave and hence have less time in which to be scattered. Note that although the equatorial parallel resonant energy is about 1 keV for $n_{eq} = 400$ el/cc, it is approximately 40 keV for $n_{eq} = 10$ el/cc.

Dependence on the geomagnetic latitude around which the resonance occurs. Figure 10 shows $\Delta\alpha_{eq}$ versus ϕ_0 for $B_w = 50$ mγ and $\alpha_{eq0} = 10°$. The curves in this case are parametric in the location of resonance. Hence the first 24 particles start from the equator at resonance, the next start at resonance at 2° latitude south of the equator, and the last start at resonance at 10° latitude. All particles travel southward away from the equator. We observe that for resonance at the equator we have a trapped mode, but as the resonance latitude is increased to 10° there is a transition to the linear mode. This is expected, since the gradient of the earth's magnetic field increases with

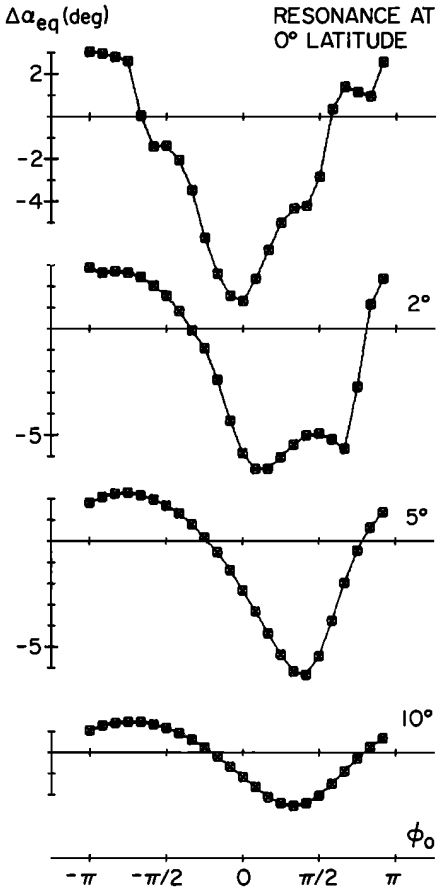

Fig. 10. Total scattering as a function of resonance point along the field line. For all cases, $L = 4$, $f = 5$ kHz, $B_w = 50$ mγ, $\alpha_{eq_c} = 10°$, and $n_{eq} = 400$ el/cc.

distance from the equator, and for high enough latitudes the effects of inhomogeneity can no longer be offset by the wave forces. Because the inhomogeneity becomes the controlling factor at higher latitudes, the shape of $\Delta\alpha_{eq}$ versus ϕ_0 returns to the linear form. Note that this behavior is limited to constant frequency waves. For waves of changing frequency, maximum interaction may occur off the equator, as suggested by *Helliwell* [1967, 1970].

Criteria for Determining Linearity

The linear theory procedure for computing the wave-induced scatterings $\dot{v}_{\parallel}$ and $\dot{v}_{\perp}$ was briefly described in previous sections. A unique feature of linear theory is that the path length over which resonance occurs is independent of wave amplitude. For instance, if an electron is in resonance ($\dot{\phi} = 0$) with the wave at some point z_1 along the magnetic field line, linear theory predicts that resonance will effectively terminate at a point z_2, defined implicitly by the approximate relation

$$\Delta\phi \simeq 1 \text{ rad} \simeq \int_{z_2}^{z_1} [\omega_H - \omega - kv_{\parallel}] \frac{dz}{v_R} \tag{8}$$

where ω_H is the electron gyrofrequency at the resonance point z_1 and $v_R = (\omega_H - \omega)/k$. It can be seen that z_2 does not depend on B_w, since in linear theory the wave-induced changes in $v_{\parallel}$ are ignored in integrating (4*c*). A rough method of establishing the validity of linear theory in any particular case is to compare the time the particle spends in the linear resonance region, $t_R = (z_2 - z_1)/v_R$, with the trapping time of the particle in the potential well of the wave, $t_T = 2\pi[(eB_w/m)kv_{\perp}]^{-1/2}$. When $t_R t_T^{-1} \ll 1$, it can be concluded that nonlinear effects will be negligible and that linear theory can be used, while if $t_R t_T^{-1} > 1$, it can be concluded that nonlinear effects must be included. The major problem with this criterion is that it is difficult to apply when $t_R t_T^{-1} \simeq 1$, since the actual nonlinear resonance time will generally exceed t_R. In this case, it is of interest to use our results to attempt to establish a more accurate method to determine the applicability of the linear theory.

The very similar behavior of the $\Delta\alpha_{eq}$ versus ϕ_0 curves as displayed in Figures 5–10 suggests that the nature of the interaction may be described by a single parameter which is a function of B_w, α_{eq_0}, n_{eq} (or k), and $\partial\omega_H/\partial z$. The controlling factor in the interaction is the variation of phase, ϕ, as given by (4*c*). Note that for all sheets considered in Figures 5–10 the set of values used for ϕ_0 is the same regardless of the values of the different parameters. For resonant particles, $\dot{\phi}_0 \simeq 0$; for nonresonant particles $\dot{\phi}_0$ is a nonzero constant. The different behavior of the sheets, whether they interact in the trapped or linear mode, is determined by the initial rate of change of $\dot{\phi}$, i.e., $\ddot{\phi}_0$. Neglecting the wave term in (4*c*) (the term proportional to $(\cos\phi/v)$, $\ddot{\phi}$ is given by (6). The first term on the right-hand side and the second term on the left-hand side of (6) represent the inhomogeneity and wave forces, respectively. We now define a quantity ρ:

$$\rho = 2k\left(\frac{eB_w}{m}\right)\tan\alpha \left[\left(3 + \frac{\omega_H - \omega}{\omega_H}\tan^2\alpha\right)\frac{\partial\omega_H}{\partial z}\right]^{-1} \tag{9}$$

This quantity is the ratio of the maximum absolute values of the wave and inhomogeneity terms in (6). Hence the value of ρ is an indication of the relative effectiveness of these terms. Note that ρ is proportional to $t_T^{-2}t_R^{-1}$. Similar analyses of the relative effects of the wave and inhomogeneity terms were used by previous authors [*Dysthe*, 1971; *Nunn*, 1974; *Karpman et al.*, 1974*a*, *b*; *Roux and Pellat*, 1976]. Note that ρ is a dimensionless quantity dependent on B_w, α (local pitch angle), k, and $\partial\omega_H/\partial z$.

We expect that ρ will be a useful quantity for differentiating between linear and nonlinear interactions. For instance, linear theory predicts that for a particle that is resonant with the wave at some point z_1 along the magnetic field line the resonance will effectively terminate at a point z_2 defined by (8). If, for any particular case, we compute the quantity ρ at z_2, we can determine whether the resonance interaction will proceed significantly beyond z_2. Thus if $\rho < 1$ at z_2, we can conclude that the wave forces are weaker than the inhomogeneity and that linear theory should apply. If $\rho > 1$ at z_2, we can conclude that the resonance interaction will proceed significantly beyond z_2, that linear theory is not appropriate, and that a full nonlinear treatment should be employed.

In practice the evaluation of ρ is simplified by the fact that for the dipole model, $\rho(z_1) \simeq \rho(z_2)$, and thus ρ can generally be simply evaluated completely in terms of the initial conditions. A slight complication occurs when the initial resonance point approaches the magnetic equator, since then $\rho(z_1) \to \infty$ as $\partial\omega_H/\partial z \to 0$. In this case, we must evaluate ρ at the point z_2. An analytic expression for z_2 can be found by using (6) and (8) in the limit $B_w = 0$ together with the parabolic approximation to the dipole field for locations close to the equator. We find that

$$z_2 = \left\{\frac{4v_R R^2}{3[3\omega_{H_0} + (\omega_{H_0} - \omega)\tan^2\alpha_0]}\right\}^{1/3}$$

where R is the geocentric radius, ω_{H_0} is the gyrofrequency at the equator, and α_0 is the initial pitch angle. This is similar to the graphical results shown in *Helliwell* [1970].

TABLE 2. Values of ρ for Different Cases

Cases	Values					
	Case 1: $\alpha_{eq} = 10°$, $L = 4$, $n_{eq} = 400$ el/cc					
B_w, mγ	1	5	7	10	30	50
ρ	0.1	0.6	0.9	1.3	3.8	6.4
	Case 2: $\alpha_{eq} = 30°$, $L = 4$, $n_{eq} = 400$ el/cc					
B_w, mγ	1	3	7	10	30	50
ρ	0.4	1.2	2.8	4.0	12.0	20.0
	Case 3: $\alpha_{eq}^{l} = 10°$, $B_w = 50$ mγ, $L = 4$					
n_{eq}, el/cc	400	200	50	10	5	1
ρ	6.4	4.5	2.3	1.0	0.7	0.3
	Case 4: $B_w = 10$ mγ, $L = 4$, $n_{eq} = 400$ el/cc					
α_{eq}, deg	1	7	10	30	70	85
ρ	0.1	0.9	1.3	4.0	10.6	8.9

Therefore for resonances at the equator, ρ can be evaluated at point z_2 using the value $(\partial\omega_H/\partial z)\,|_{z_2} \simeq 9\omega_{H_0}(z_2/R^2)$. For the parameters of Table 1,

$$z_2 \simeq 576[3 + 0.63 \tan^2 \alpha_0]^{-1/3} \quad \text{km}$$

and using these, we obtain

$$\left.\frac{\partial \omega_H}{\partial z}\right|_{z_2} = 6.86 \times 10^{-1}[3 + 0.63 \tan^2 \alpha_0]^{-1/3} \quad \text{rad/km}$$

The quantity $\rho(z_2)$ can be determined simply in terms of initial values by making use of the fact that $\omega_H(z_2) \simeq \omega_{H_0}$ and $\alpha(z_2) \simeq \alpha_0$. Thus two important features of the quantity ρ are that (1) its value can be used to determine when linear theory is appropriate and (2) it can be evaluated simply in terms of the initial conditions alone.

In the following we demonstrate that the transitions from the linear to the quasi-trapped mode in Figures 5–10 occur at or near the $\rho \simeq 1$ threshold.

In Table 2 we give the values of ρ for the cases covered in Figures 5–10. First, consider the wave amplitude dependence as illustrated in Figure 5*a* for $\alpha_{eq_0} = 10°$. Case 1 in Table 2 gives ρ for different B_w. From Figure 5*a* we see that significant deviations of the $\Delta\alpha_{eq}$ versus ϕ_0 curves from a linear near-sinusoidal variation start at about $B_w = 7$ mγ. Since $\rho \simeq 0.9$ for 7 mγ, we can loosely conclude that linear theory fails for $\rho > 1$.

Case 2 in Table 2 shows the corresponding values of ρ for the different wave amplitudes of Figure 5*b*, for which $\alpha_{eq_0} = 30°$. From that figure it is evident that a large deviation from the linear mode is seen for $B_w > 3$mγ compared to an almost linear result for $B_w = 1$ mγ. Hence we can say that the deviation from linear theory starts at $B_w \simeq 2$–3 mγ. We see from case 2 that $\rho \simeq 1$ for these values. Therefore $\rho = 1$ again is a reasonably good indication of the point beyond which linear theory becomes inaccurate.

The value of ρ for the different n_{eq} values of Figure 9 is given in case 3 in Table 2. We see from Figure 9 that linear theory applies for $n_{eq} \leq 10$ el/cc.

Figure 10 shows $\Delta\alpha_{eq}$ versus ϕ_0 for different resonance points along the field line. It is evident from the figure that we have a well-defined linear mode for resonances at latitudes of $\geq 10°$. For particles resonant at 10°, $\rho(z_1) \simeq \rho(z_2)$, and we can use $\partial\omega_H/\partial z$ at 10° latitude for computing ρ. This gives $\rho = 0.71$. Note that the $\Delta\alpha_{eq}$ versus ϕ_0 curve for 10° latitude is very nearly linear, whereas the one for 5° latitude is different from a linear mode. Here we have $\rho = 1.7$ for resonance at 5° and $\rho = 1.0$ at 7.5° latitude. Therefore we see that $\rho \simeq 1$ is again a valid threshold point for determining linearity.

As a final test of our criterion we use the 'experimental data' given in Figure 8. Case 4 in Table 2 gives values of ρ for the α_{eq_0} values used in that figure. The deviation from the linear mode starts around $\alpha_{eq_0} = 7°$ (this case is not illustrated in Figure 8) and $\rho \simeq 0.9$ at that point, again very close to the $\rho \simeq 1$ criterion which was established above. The sharpness of the minima for $\alpha_{eq} = 5°$ given in Figure 8 is not so much due to the deviation from linearity as it is due to the wave term in (4*c*), since at that point, $\Delta\alpha_{eq} \simeq \alpha_{eq_0}$.

As we examine case 4 in Table 2 we see that ρ reaches at maximum at about $\alpha_{eq_0} = 50°$. The pitch angle dependence of ρ is clear from (9). The maximum of this function occurs when $((\omega_H - \omega)/\omega) \tan^2 \alpha = 9$. For the parameters of Table 1, this maximum is at $\alpha \simeq 75°$. From Figure 8 we see that for $\alpha_{eq_0} > 60°$ the $\Delta\alpha_{eq}$ versus ϕ_0 curves start to shrink while remaining in the trapped mode. This correlation between case 4 in Table 2 and Figure 8 (i.e., the fact that both ρ and the scattering reach their maxima for $\alpha \simeq 65°$–$75°$) is very interesting. It indicates that not only is ρ useful as a threshold criteria for determining linearity, but also its absolute magnitude may be a direct indication of the amount of scattering. We have determined that ρ can be used as an empirical parameter for easy computation of the scattering coefficients for the trapped mode. Our results on this problem will be reported in a later paper.

With the above results and comparisons we have established the following:

1. The quantity ρ can be used to determine whether the linear theory is applicable for given interaction parameters. The procedure is to compute ρ for the parameters of the problem at hand.
2. For $\rho \ll 1$ ($\rho < 0.7$), linear theory results are close to those of the full nonlinear analysis.
3. For $\rho \gg 1$ ($\rho > 3$) we have a trapped mode, and the linear theory is not applicable.
4. The linear theory results begin to deviate significantly from those of the full nonlinear analysis for $\rho > 1$.

The criteria established above use only the initial values of the parameters. Therefore one need not compute the particle trajectories in order to use this criterion. This fact makes the method very useful in determining whether one can use a simple linear analysis for the interaction of a particle with a given pitch angle at any point along the field line with a wave of any frequency and wave amplitude.

Previous authors, for example, *Ashour-Abdalla* [1972], have used linear theory without quantitative justification. For the parameters of *Ashour-Abdalla* [1972] and for equatorial interactions we compute $\rho = 0.6$ for $\alpha_{eq_0} = 10°$, $\rho = 1.7$ for $\alpha_{eq_0} = 30°$, and $\rho = 2.5$ for $\alpha_{eq_0} = 50°$. Note that none of these values

for ρ satisfy $\rho \ll 1$, which guarantees safe application of linear theory. Furthermore, for $\alpha_{eq_0} > 30°$, $\rho > 1$. For this reason we believe that the scattering coefficients given in that paper for resonances close to the equator (within 500–1000 km) are inaccurate for high pitch angles.

5. Precipitated Flux From a Full Distribution of Particles

In this section we present an application of our simulation for the calculation of the one-pass precipitated electron flux for a particular case.

Simulation of the Full Distribution

The full distribution of particles is simulated by a large number of test particles. For energetic particles adiabatically trapped in the earth's magnetic field, the particle population in every flux tube can be represented by an equatorial distribution function $f_{eq}(v_{\|eq}, \alpha_{eq})$.

From this point on, we drop the subscript 'eq' for the purpose of simplifying the text. Unless otherwise mentioned, all quantities $v_\|$ and α in this section represent equatorial values. We have chosen to work with the distribution function in the $v_\perp$-α space as opposed to v-α or $v_\|$-$v_\perp$ spaces. This formulation is convenient for our simulation, since it directly shows the pitch angle scattering along the α axis and makes it possible to uniquely identify each $v_\|$ mesh point with a resonance location through (1). The velocity space volume element in terms of $v_\|$ and α is $v_\|^2[(\sin\alpha)/(\cos^3\alpha)]\, d\alpha\, dv_\|\, d\phi$.

For a given field line and a given wave, only a limited portion of the total particle population represented by this distribution will resonate with and hence be scattered significantly by the wave. Therefore in our simulation we need only consider that limited portion of the distribution. The α_{min} is determined by the loss cone. For given plasma and wave parameters, α_{max} is determined by the nature of the problem. For example, for the computation of the one-pass precipitated flux an $\alpha_{max} < \pi/2$ can always be found such that for the given parameters, particles with $\alpha > \alpha_{max}$ cannot be scattered into the loss cone at the first encounter with the wave. On the other hand, if one wishes to consider the steady state scattering problem, it is necessary to take $\alpha_{max} \simeq 90°$, since in this case multiple scatterings can bring high pitch angle particles down to the loss cone. The $v_{\|min}$ is determined by the resonance velocity at the equator. Particles with parallel velocities lower than $v_{\|min}$ do not resonate with the wave at any point along the field line. The upper limit $v_{\|max}$ is determined by the fact that particles with higher $v_\|$ resonate at points so far down the field line that the scattering produced is less than one half of the pitch angle mesh size used in the calculations. That is, for given parameters we can find a $v_{\|max}$ such that the scattering for particles with $v_\| > v_{\|max}$ will be negligible and need not be considered. Once the shaded area is determined, this region in the $v_\|$-α space is divided into a number of mesh points. Each mesh point is identified with a pair $v_\|$ and α. The value of the distribution at each mesh point is $f(v_\|, \alpha)$. Figure 11*b* illustrates such a representation of the distribution function. For purposes of illustration we have chosen a uniform distribution with a sharp cutoff at the loss cone. The mesh sizes in $v_\|$ and α are $\Delta v_\|$ and $\Delta\alpha$, respectively. The number density of particles with parallel velocities $v_\| \pm (\Delta v_\|/2)$ and pitch angles $\alpha \pm (\Delta\alpha/2)$ is given by

$$\Delta N = 2\pi f(v_\|, \alpha) v_\|^2 \frac{\sin\alpha}{\cos^3\alpha} \Delta\alpha\ \Delta v_\| \tag{10}$$

where the factor 2π is due to integration over the cyclotron phase ϕ. We assume a uniform distribution in ϕ.

In our formulation each such population $(v_\| \pm (\Delta v_\|/2), \alpha \pm (\Delta\alpha/2))$ of particles is represented by test particles with parallel velocity $v_\|$ and pitch angle α. When the mesh sizes $\Delta v_\|$ and $\Delta\alpha$ are chosen adequately small, the motions of these test particles accurately represent the motion of all particles with $v_\| \pm (\Delta v_\|/2)$ and $\alpha \pm (\Delta\alpha/2)$.

Since the gyroresonant interaction is highly dependent on initial phase, we use 12 test particles uniformly distributed in ϕ for each mesh point. In that case, each test particle with initial equatorial values $v_{\|0}$, α_0, and a phase ϕ_0 represents the population of particles with $v_\| = v_{\|0} \pm (\Delta v/2)$, $\alpha = \alpha_0 \pm (\Delta\alpha/2)$, and $\phi = \phi_0 \pm (\pi/12)$. The actual number density of such particles is

$$\frac{\Delta N}{12} = f(v_{\|0}, \alpha_0)\, v_{\|0}^2 \frac{\sin\alpha_0}{\cos^3\alpha_0} \Delta\alpha\, \Delta v_\| \left(\frac{\pi}{6}\right) \tag{11}$$

The next step is to simulate the interaction for the test particle. The test particle is allowed to go through the complete interaction as described in section 3. For a CW wave which has equal intensity over the whole field line the equations of motion for the test particle are integrated from the point N′ in the northern hemisphere where $\epsilon = (v_\| - v_R)/v_R = -0.03$ to the point S′ in the southern hemisphere where $\epsilon = +0.05$ (see Figure 2*b*). At the end of the interaction the test particle has acquired a new equatorial velocity and pitch angle, namely, $v_{\|F}$ and α_F (F for final) and must now be identified with the mesh point $(v_{\|F}, \alpha_F)$. This means in effect that all the particles represented by this test particle have acquired parallel velocity and pitch angle values in the ranges $v_{\|F} \pm (\Delta v_\|/2)$ and $\alpha_F \pm (\Delta\alpha/2)$, respectively. In order to conserve the total number density of particles in the system the following changes must be made in the values of the distribution function at $(v_{\|0}, \alpha_0)$ and $(v_{\|F}, \alpha_F)$:

$$f_{new}(v_{\|0}, \alpha_0) = f_{old}(v_{\|0}, \alpha_0) - \tfrac{1}{12} f_{old}(v_{\|0}, \alpha_0) \tag{12}$$

$$f_{new}(v_{\|F}, \alpha_F) = f_{old}(v_{\|F}, \alpha_F) + \tfrac{1}{12} f_{old}(v_\|, \alpha_0) \cdot \frac{v_{\|0}^2(\sin\alpha_0)/(\cos^3\alpha_0)}{v_{\|F}^2(\sin\alpha_F)/(\cos^3\alpha_F)} \tag{13}$$

Using 12 such test particles for each mesh point and repeating the procedure for every mesh point, we obtain the perturbed distribution.

Figure 11*c* shows an illustrative sketch of the perturbed distribution. After one pass of the wave the empty loss cone of the initial distribution is partly filled. The total number of precipitated particles and the precipitated flux can be obtained by properly integrating the perturbed distribution over $v_\|$ and α. This is done in detail for the sample computation of the next section.

Computation of Flux for a Particular Case

As an application of the technique described above, we compute the precipitated particle flux for a particular case. The medium and wave parameters given in Table 1 are used for different wave intensities. For these computations a pitch angle mesh size of 0.5° is used, with 60 mesh points in pitch angle covering from $\alpha = 0°$ to 30° in 0.5° steps. Pitch angles greater than 30° were not considered because even for the largest wave intensity used in the calculations ($B = 50$ mγ) no particles with $\alpha_0 > 30°$ are scattered into the loss cone during one pass through the wave. A variable mesh size in $v_\|$ is used with mesh size increasing with $v_\|$. About 85 bins in $v_\|$ covering the range from $v_\| = 1.87 \times 10^4$ km/s (parallel energy of ~1 keV) to $v_\| = 6.01 \times 10^4$ km/s (parallel energy of ~10 keV)

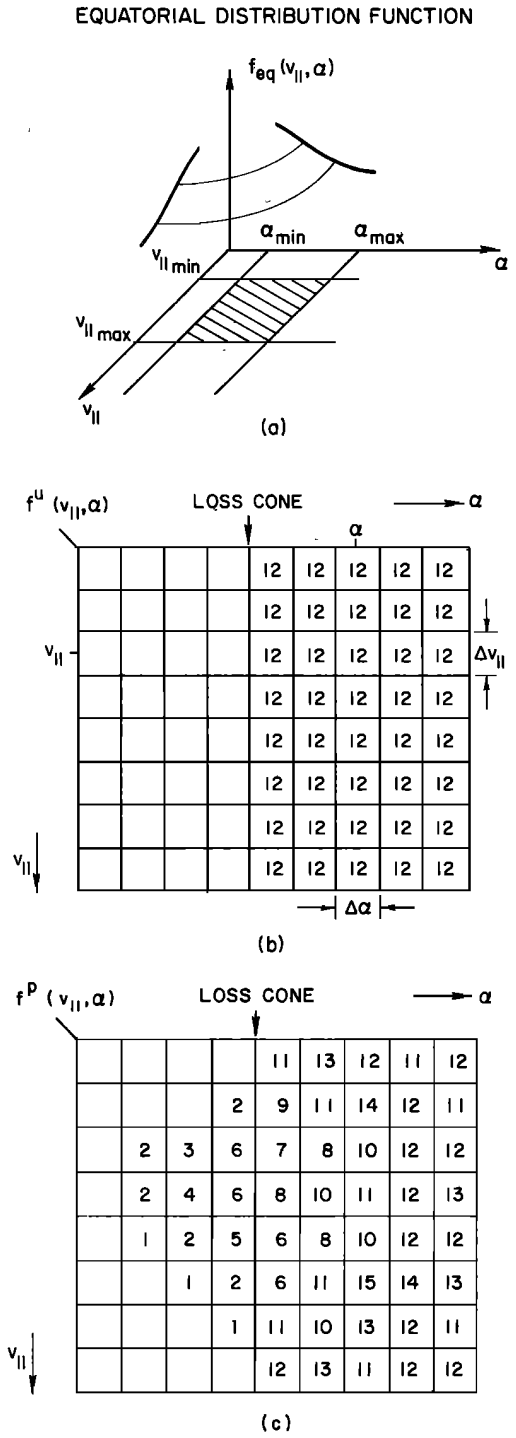

Fig. 11. Simulation of the distribution function. (*a*) The general distribution: The shaded area is the portion that will be significantly affected by the wave. (*b*) Unperturbed distribution: In this illustration a uniform distribution with $f(v_{||}, \alpha) = 12$ above the loss cone, and $f(v_{||}, \alpha) = 0$ in the loss cone is shown. (*c*) Perturbed distribution.

were used with mesh sizes ranging from 0.1 to 2.8%. The resonance points are at the equator for the 1-keV particles and at ±20° for particles at 10-keV parallel energy (assuming $\alpha_{eq} \simeq 15°$). All together about 40,000–50,000 test particles are used for each computation.

The initial unperturbed distribution is assumed to be of the form

$$f(v, \alpha) = \frac{A}{v^4} g(\alpha) \qquad \alpha > \alpha^{lc}$$
$$f(v, \alpha) = 0 \qquad \alpha < \alpha^{lc} \tag{14}$$

where A is a constant, $g(\alpha)$ is some function of pitch angle, and α^{lc} is the halfwidth of the loss cone. The energy variation of $f(v, \alpha)$ is in reasonable agreement with experimental measurements of the trapped low-energy fluxes in the magnetosphere [*Schield and Frank*, 1970]. In our computations we consider two different distribution functions, (1) an isotropic distribution for which $g(\alpha) = g_1(\alpha) = 1$ and (2) an anisotropic distribution with $g(\alpha) = g_2(\alpha) = 0.2 \sin^{0.2}\alpha + 0.8 \sin^{12}\alpha$. The two distributions have the same value at $\alpha = 90°$, and they are sketched in Figure 12. Both isotropic and anisotropic distributions have been measured in the magnetosphere [*Lyons and Williams*, 1975]. The particular anisotropic distribution of Figure 12*b* was reported by *Anderson* [1976] and is considered to be highly anisotropic.

Note that both distributions in Figure 12 are essentially flat for $0° < \alpha < 30°$. In our computations of the precipitated flux due to one pass through the wave we consider only particles with $\alpha < 30°$. Therefore for the purposes of the computer simulation both distributions can be treated as isotropic, but with different flux levels just above the loss cone.

Isotropic case. In this case the initial unperturbed distribution is

$$f(v_{||}, \alpha) = \frac{A \cos^4\alpha}{v_{||}^4} \qquad \alpha \gtrsim \alpha^{lc}$$
$$f(v_{||}, \alpha) = 0 \qquad \alpha \lesssim \alpha^{lc} \tag{15}$$

With this as the input distribution, the test particle simulation described in the last section is carried out, and the perturbed

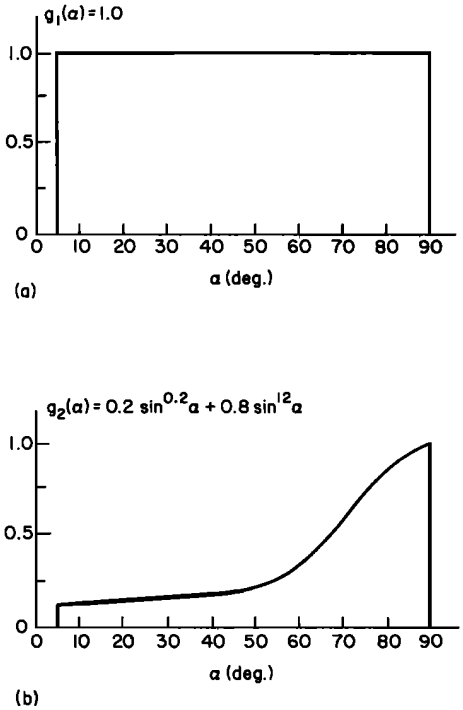

Fig. 12. Pitch angle dependence of the two distribution functions used in the calculations: (*a*) an isotropic distribution and (*b*) an anisotropic distribution.

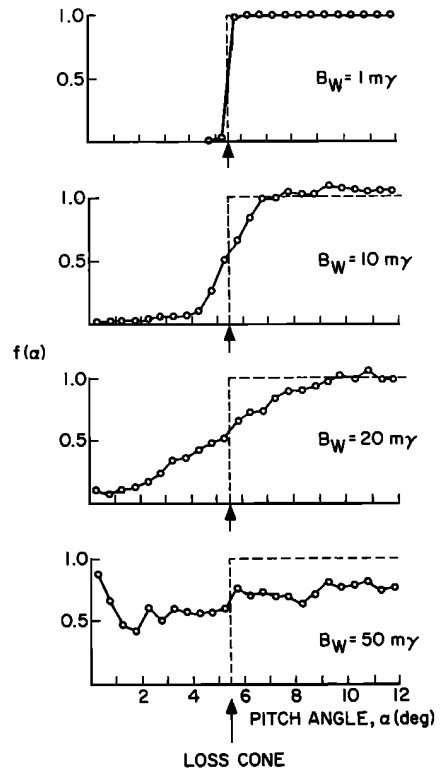

Fig. 13. Normalized particle distribution $f(\alpha)$. The dashed lines represent the unperturbed distribution which is isotropic in pitch angle. The solid lines represent the one-pass perturbed distribution. The number density in any given range $d\alpha$ is equal to $f(\alpha) \sin \alpha \, d\alpha$.

distribution is obtained. The output of this computation is the value of the perturbed distribution at the $30 \times 85 = 2550$ mesh points, covering from $\alpha = 0°$–$30°$ and $v_{\|} = v_k$ to $v_{\|} = 10^{1/2} v_k$, where $v_k = 1.9 \times 10^7$ m/s is the velocity corresponding to 1-keV energy, such that $0.5 m v_k^2 = 1$ keV.

In the following we concentrate on the 1- to 2-keV total energy band. First, in order to show the wave-induced pitch angle perturbations of the distribution function we integrate the distribution over $v_{\|}$ to obtain

$$f(\alpha) = 2\pi \int_{v_{\|} = v_k \cos\alpha}^{v_{\|} = 2^{1/2} v_k \cos\alpha} f(v_{\|}, \alpha) v_{\|}^2 \, dv_{\|} \qquad (16)$$

where we again assume uniform distribution over ϕ.

Figure 13 shows the normalized distribution $f(\alpha)$ versus α for different wave intensities. The dashed lines show the unperturbed distribution which is isotropic above the loss cone, as is clear from (15). The solid lines show the one-pass perturbed distribution. Note again that only the 1- to 2-keV total energy band is considered. The integral given in (16) is easily carried out with the computer, using the mesh point values $f(v_{\|}, \alpha)$ and $\Delta v_{\|} \simeq dv_{\|}$ and approximating the continuous integral by a weighted sum of finite numbers of values of $f(v_{\|}, \alpha)$.

For $B_w = 1$ mγ the perturbations are small, and only a small percentage of the particle population from the range just above the loss cone has been precipitated. For $B_w = 10$ mγ the loss cone is partly filled with particles scattered down from higher pitch angles. Most of the particles scattered into the loss cone originally had pitch angles in the 2°–3° range just above the loss cone. For $B_w = 20$ mγ and 50 mγ, the number of precipitated electrons is higher than for $B_w = 10$ mγ, and there are more particles deeper into the loss cone. Also, by observing the distribution at pitch angles above the loss cone we see that contributions to the loss cone population come from a wider range of pitch angles for higher wave intensities.

The total number density of precipitated electrons in the 1- to 2-keV energy range is given by

$$N_T = 2\pi \int_0^{\alpha^{lc}} \int_{v_{\|} = v_k \cos\alpha}^{2^{1/2} v_k \cos\alpha} \cdot f(v_{\|}, \alpha) v_{\|}^2 \frac{\sin\alpha}{\cos^3\alpha} \, dv_{\|} \, d\alpha [L^3(1 + 3\sin^2\lambda_t)^{1/2}] \qquad (17)$$

where α^{lc} is the loss cone angle (5.5° at equator for $L = 4$) and the last factor $L^3(1 + 3\sin^2\lambda_t)^{1/2}$ describes the convergence of the field lines which gives a reduced flux tube cross section at the ionosphere as compared to that at the equator. In this case, λ_t would be the latitude at which the $L = 4$ field line crosses ionospheric heights, i.e., $\lambda_t \simeq 60°$. Note that all evaluations in the integrand are done using equatorial values, whereas N_T is the precipitated number density at the ionosphere. The precipitated energy deposition rate in the same range is

$$Q = 2\pi \int_0^{\alpha^{lc}} \int_{v_{\|} = v_k \cos\alpha}^{2^{1/2} v_k \cos\alpha} f(v_{\|}, \alpha) v_{\|}^2 \frac{\sin\alpha}{\cos^3\alpha} \left(\frac{1}{2} m \frac{v_{\|}^2}{\cos^2\alpha} \right) \cdot (v_{\|}) \, dv_{\|} \, d\alpha [L^3(1 + 3\sin^2\lambda_t)^{1/2}] \qquad (18)$$

Both integrations (17) and (18) reduce to finite weighted sums in our computer formulation. With the perturbed distribution $f(v, \alpha)$ obtained at the mesh points, the energy deposition rate Q is evaluated without difficulty. For $B_w = 10$ mγ we obtain

$$Q = 4.2 \times 10^{-10} A \quad \text{erg/cm}^2 \text{ s} \qquad (19)$$

where A is the proportionality constant in (14) and (15). The constant A can be evaluated in terms of measured number density using (14). We find that $A = 5.2 \times 10^8 N_e$, where N_e is the number density of isotropically distributed electrons in the 1- to 2-keV energy range. Thus $Q = 0.2 N_e$ ergs/cm² s for $B_w = 10$ mγ. Figure 14 shows the energy deposition rate as a function of wave intensity. The dashed straight line gives the results predicted on the basis of linear theory. The vertical scale on the left is normalized to $|N_e|$. The one on the right is normalized to $|\Phi_1|$, the differential energy spectrum for $\alpha \simeq 90°$ particles with ~1-keV energy. As can be seen from Figure 14, the precipitated flux increases with wave intensity for $B_w \leq 40$ mγ and begins to saturate for $B_w \gtrsim 40$ mγ. The variation should be compared to that of the rms scattering given in Figure 7.

Schield and Frank [1970] have reported measurements of low-energy electrons on the Ogo 3 satellite. Figure 6 of their paper indicates number densities of 3 el/cc in the energy range 750 eV $\lesssim E \leq 50$ keV inside the plasmapause at $L \simeq 4$. Figure 4 of the same paper indicates that number density varies as v^{-4} with velocity (E^{-2} with energy). Using this type of energy dependence, we obtain $N_e = 1$ el/cc in the 1- to 2-keV range. Using this value for N_e gives a precipitated flux of $Q = 0.22$ erg/cm² s for $B_w = 10$ mγ wave intensity.

The energy deposition rate can also be expressed in terms of the differential energy spectrum Φ [*Schield and Frank*, 1970]. Using (15), we find $A = 2\Phi_1$, where Φ_1 is the differential energy spectrum in el/cm² sr s keV for the ~1-keV electrons. Similarly, we find $Q = 10^{-9}\Phi_1$ erg/cm² s for $B_w = 10$ mγ.

A more recent measurement of low-energy electron fluxes on the Explorer 45 (S^3) satellite was reported by *Anderson* [1976]. For disturbed premidnight conditions and for ~1-keV

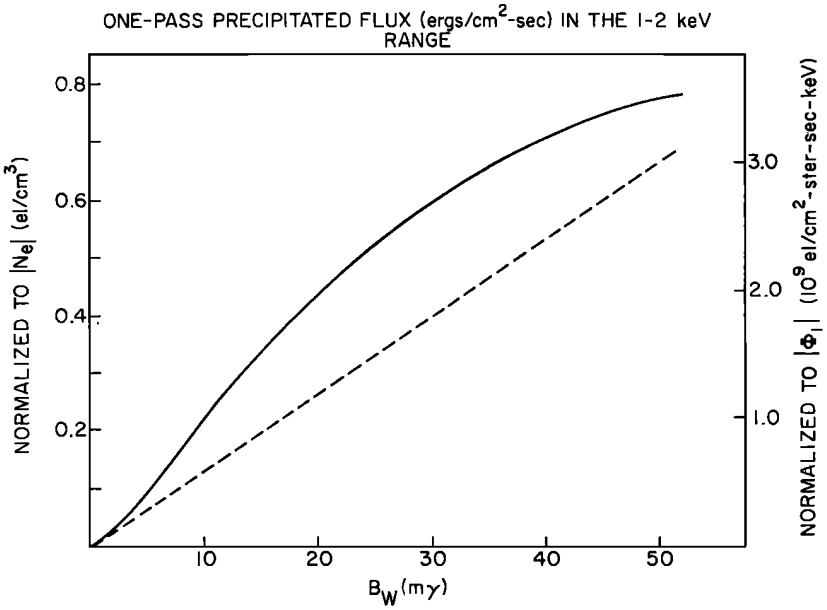

Fig. 14. The one-pass precipitated flux in the 1- to 2-keV range as a function of wave intensity. This result is for an isotropic distribution. The vertical scale on the left gives the flux (ergs/cm² s) normalized to $|N_e|$, where N_e is the electrons per cubic centimeter in the 1- to 2-keV range. The one on the right gives flux normalized to $|\Phi_1|$, the differential energy spectrum in el/cm² sr s keV, for ~1-keV electrons at $\alpha \simeq 90°$.

electrons with isotropic distributions the energy spectrum Φ_1 is of the order of $\sim 10^8$ el/cm² sr s keV, resulting in an energy deposition rate of $Q \simeq 0.1$ erg/cm² s.

Anisotropic case. For this case the pitch angle dependence is $g(\alpha) = 0.2 \sin^{0.2}\alpha + 0.8 \sin^{12}\alpha$, as plotted in Figure 12. For $\alpha \lesssim 30°$ this distribution can be approximated by

$$f(v_{\|}, \alpha) \simeq (0.15)A \frac{\cos^4 \alpha}{v_{\|}^4} \qquad \alpha^{lc} < \alpha \lesssim 30°$$
$$f(v_{\|}, \alpha) = 0 \qquad \alpha \leq \alpha^{lc} \tag{20}$$

When the distribution given by (20) is used as the initial distribution in our simulation, the results should be the same as those for the distribution given by (15) within a factor 0.15. Therefore for this anisotropic case and for $B_w = 10$ mγ, $Q = 6.35 \times 10^{-11} A$ erg/cm² s, where A is the proportionality constant in (14) or (20).

The differential energy spectrum for the anisotropic distribution is $\Phi = (A/2E)[0.2 \sin^{0.2}\alpha + 0.8 \sin^{12}\alpha]$, where E is the energy. Substituting $E \simeq 1$ keV and $\alpha = 90°$, we obtain $A = 2\Phi_1$, where Φ_1 is the spectrum in el/cm² sr s keV for ~1-keV electrons at $\alpha = 90°$. That this is the same relation as the isotropic case is not surprising, since the two distributions used in the calculations (Figure 12) were chosen to have the same value at $\alpha = 90°$. This gives $Q = 1.3 \times 10^{-10}\Phi_1$ erg/cm² s for $B_w = 10$ mγ.

We again use the data reported by Anderson to find absolute values for the energy deposition rate. For 1-keV electrons with anisotropic distributions similar to that of the second panel of Figure 5 the differential energy spectrum for $\alpha = 90°$ particles is $\Phi_1 \simeq 10^8$ cm^{-2} sr^{-1} s^{-1} keV^{-1}. Hence the energy deposition rate $Q = 1 \times 10^{-2}$ erg/cm² s.

These values show that the one-pass fluxes in the 1- to 2-keV range precipitated by a 10-mγ CW signal at 5 kHz can be as much as 1×10^{-2} to 0.2 erg/cm² s depending on the anisotropy of the distribution function. Such fluxes are well within the resolution of most particle detectors. The intensities approach that of a moderate aurora.

Leverage

In the cyclotron resonance interaction, large pitch angle changes induced by the wave on the particles do not necessarily require a large amount of energy exchange. The basic reason for this is the fact that the wave perturbations are caused mainly by the wave magnetic field which changes the direction of momentum (i.e., pitch angle) of the particle without changing the energy much.

We have shown in the previous section that energy fluxes of as much as 0.2 erg/cm² s can be precipitated by waves of 10-mγ intensity. It is instructive to compare the energy density of the precipitated flux and that of the input wave and compute the leverage involved in the wave-induced precipitation process.

For longitudinal whistler mode propagation the wave Poynting flux is given by $|P| = (c/n\mu_0)|B_w|^2$, where B_w is in milligammas, c is the velocity of light, n is the wave refractive index, and μ_0 is the permeability of free space. For the parameters of Table 1, $n \simeq 40$ at the equator. Using this together with $B_w = 10$ mγ, we obtain the wave energy flux $|\mathbf{P}| \simeq 6 \times 10^{-9}$ W/m². A precipitated flux of 0.2 erg/cm² s is equivalent to an energy density of about 0.2×10^{-3} W/m². This shows that the leverage involved in this interaction is $\sim 10^5$, or 50 dB. Therefore significant particle fluxes can be precipitated by waves of moderate intensity.

The above calculations relate to the energy densities. We can also consider the total input and output power and compute the leverage on an integrated basis. The Siple VLF transmitter operates with a total radiated power ranging from 100 W to 1 kW. If we assume that the precipitated flux is distributed over an area of 100-km radius, the total precipitated power is $\sim 10^7$ W, a factor of $\sim 10^5$ larger than the radiated power. Hence the power leverage of the interaction is ~50 dB. The input power of the transmitter is ~100 kW. Since an output of $\sim 10^7$ W is

obtained, the net power gain is ~20 dB. The source of this extra power is of course the energy of the trapped energetic particles.

Note that these numbers are obtained by considering only the 1- to 2-keV energy band. The same wave will also precipitate particles with higher energies. Therefore the total leverage and the power gain will be somewhat larger than those computed above. Furthermore, we have implicitly assumed that 100 kW of input power is necessary for generating a 10-mγ signal. This is very likely to be an overestimate. Recent results from a power step (up and down) experiment using the Siple transmitter have shown that magnetospheric signals of the same intensity can at times be produced with lower power levels, so long as this level is above a threshold value.

6. Conclusions and Discussion

We have analyzed the nonlinear gyroresonance interaction between energetic electrons and coherent VLF waves in the magnetosphere. In our study we have focused on magnetospheric parameters appropriate for the $L = 4$ field line. This is the approximate location of the Siple VLF transmitter in Antarctica, the source of many of the data concerning nonlinear interactions between coherent VLF waves and energetic electrons in the magnetosphere.

We have used a computer simulation of the full nonlinear equations of motion for energetic particles interacting with a longitudinal whistler mode wave in an inhomogeneous magnetoplasma. We have studied in detail interaction of single particles and a full distribution of particles with a given wave. The interaction of a full particle distribution is determined by using a test particle approach. In this approach, in order to estimate the perturbation of the full distribution, the complete trajectories of a representative number of particles distributed appropriately in phase space are computed.

We have shown how the nonlinear pitch angle scattering varies as a function of particle pitch angle, wave amplitude, cold plasma density, and resonance position along the magnetic field line. We have compared the nonlinear theory with the well-known linear theory and have derived a quantitative criterion for determining the applicability of linear theory in any particular case. In particular, our results indicate that nonlinear effects are significant for wave amplitudes as low as 3 mγ for a 5-kHz signal near the magnetic equatorial plane at $L \simeq 4$.

Our full distribution calculations show that significant precipitated energetic electron fluxes can be produced with moderate strength VLF waves. For example, our results indicate that at $L \simeq 4$ a 10-mγ, 5-kHz wave can produce a precipitated energy flux of 1- to 2-keV electrons of as much as 10^{-1} erg/cm² s, the exact value depending upon the value of the energetic electron distribution function near the loss cone. We have shown that significant leverage is involved in the wave-induced particle precipitation process. Typically, the energy density of the precipitated flux is 50–60 dB higher than that of the wave. We have computed the ionospheric perturbations due to these precipitated fluxes and have shown that significant density enhancements can be induced in the nighttime ionosphere.

Measurement of the Precipitated Flux

Assuming that our calculations of wave-induced precipitation are correct, the question arises as to how the precipitation flux itself or the resulting ionospheric perturbations can be detected.

The most direct method of detection is to employ satellite particle detectors. However, this method has drawbacks at both high and low altitude. At high altitude near the magnetic equatorial plane the precipitating fluxes are less intense, and the particle detectors must be directed into the loss cone. Since the half angle of the loss cone is very small (~5° at $L = 4$), the pointing accuracy of the detector must be high, and its angular resolution must be at least equal to the loss cone half angle. At low altitude (~500 km) the loss cone half angle approaches 90°, and the detector pointing accuracy and angular resolution are not critical parameters. However, the satellite velocity is high (~7 km/s), and the region of precipitation may be small (~100-km scale), so that the time available for flux measurements may be severely limited.

A second method involves the use of photometers at ground stations such as Siple Station, Antarctica. If an experiment lasts for several weeks, there is a good probability that the precipitation region will sometimes be located within 100 km of the transmitter. In this case, enhanced photoemission from the atmosphere should be readily detectable on the ground near the transmitter if the precipitated flux exceeds 0.01 erg/cm² s. Recent photometer measurements at Siple Station have shown that significant enhancements in the photometer output can be produced by precipitation induced by VLF whistler mode noise bursts at 2–4 kHz (J. Doolittle, private communication, 1977).

A third method makes use of precipitation-induced modification of the D region. Energetic electrons are precipitated into the atmosphere, penetrate the D layer, and change the properties of the earth-ionosphere wave guide. These changes are detected by monitoring the amplitude and/or phase of VLF waves propagating over long distances (~1000 km) in the earth-ionosphere wave guide. This type of modification has already been observed to occur as a result of precipitation of 30-keV electrons by whistlers [*Helliwell et al.*, 1973]. It appears that the same type of interaction should take place whether the coherent input wave is a signal from a VLF transmitter, a natural whistler, or a discrete emission.

Still another method is the use of high-altitude balloons to detect Bremsstrahlung X rays produced by the precipitating electrons. For example, *Rosenberg et al.* [1971] have measured one-to-one correlation between VLF emissions and bursts on the balloon X ray measurements.

Additional methods of precipitation detection include riometer and ionosonde techniques.

Intensity of Coherent Waves in the Magnetosphere

Although we have presented our results for a wide range of wave intensities, we have stressed the results for a 10-mγ wave amplitude. Evidence in support of this value comes predominantly from high-altitude satellite data. For instance, the amplitude of the VLF stations NAA (17.8 kHz) and NPG (18.6 kHz) were measured by a VLF experiment on the high-altitude satellite Ogo 1 when this satellite crossed the magnetic field lines linking the transmitters ($L \simeq 3$). It was found that 10 mγ was a representative amplitude for the transmitter signals near the magnetic equatorial plane [*Heyborne*, 1966].

VLF waves in the magnetosphere produced by the relatively low power (output of ≥1 kW) Siple Station transmitter have frequently been observed on satellites [*Inan et al.*, 1977]. In one representative case a wave amplitude of 0.3 mγ was measured when the satellite (Imp 6) was at a latitude of 20°S on the field line ($L \sim 4$) linking the transmitter. Since the satellite intercepted the signal on the transmitter side of the equator and

before the signal had traveled once over the field line, it was concluded that the wave was unamplified. Considering the commonly observed 30-dB amplification of VLF signals in the magnetosphere [*Helliwell and Katsufrakis,* 1974], the signal intensity at the equator could have been as high as 9 mγ. Thus it may be the case that even low-power transmitters can produce wave amplitudes of 10 mγ near the magnetic equatorial plane. The amplitude of the naturally occurring highly coherent VLF signals known as 'chorus' has been measured on a number of satellites [*Burtis and Helliwell,* 1976; *Tsurutani and Smith,* 1974; *Taylor and Gurnett,* 1968]. The amplitude of these quasi-coherent signals near 5 kHz has typically been found to lie in the range 2–20 mγ.

Furthermore, because of the predicted high radiation efficiency of dipole and loop antennas at VLF frequencies in the ionosphere and magnetosphere [*Wang and Bell,* 1972], it appears possible to produce an unamplified 10-mγ wave near the magnetic equatorial plane on the L = 3–5 field lines using a 1-kW VLF transmitter on a low-altitude satellite.

Similarly, a high-altitude satellite-based VLF transmitter of 1-kW output operating within a few thousand kilometers of the magnetic equatorial plane could be expected to produce a wave field exceeding 100 mγ within 1000 km of the equatorial plane.

Thus a 10-mγ amplitude is representative of highly coherent VLF wave types that can presently be found, or that may be introduced in the future, in the magnetosphere. When these waves are present, strong pitch angle scattering of energetic electrons can be expected. Details of this scattering will depend upon the spectral form of the coherent wave. Our present results, which are based on the assumption of a fixed frequency wave, are meant to apply primarily to the case of VLF wave injection experiments involving fixed frequency inputs near the L = 4 field lines. These experiments can be either ground, space station, or satellite based. However, our results can also be applied to the case of pitch angle scattering by chorus and whistler elements so long as the wave frequency changes slowly with time.

Self-Consistent Field Structure

The particle scattering calculations presented in the main body of this report have not directly included the effects on the wave of the electromagnetic fields generated by the perturbed energetic particles. In effect we assume either that the currents stimulated in the energetic particle population do not lead to significant damping or amplification of the wave or that this effect has been included in the model chosen for the wave field structure. It is assumed, in other words, that the wave field is known as a function of space and time.

It is not within the scope of this paper to consider how the wave function is established along the path of integration. The propagation and dispersion of VLF waves in the magnetosphere are mainly controlled by the cold plasma. However, it is widely believed that VLF waves are amplified or damped as a result of interactions with energetic electrons in the magnetosphere. One of the wave particle interactions to which VLF wave amplification and emission generation in the magnetosphere are most commonly attributed is the cyclotron resonance interaction. The wave amplification or damping in this type of interaction is due to the wave's phase bunching of the energetic particles which creates a net current [*Helliwell,* 1967, 1970; *Helliwell and Crystal,* 1973; *Nunn,* 1974]. Experimental and theoretical evidence indicates that the source of generation of cyclotron growth is in the equatorial plane [*Helliwell,* 1967; *Helliwell and Katsufrakis,* 1974; *Tsurutani and Smith,* 1974]. Furthermore, there is evidence that the growth is temporal in nature and occurs within ~500 km of the equator. Since for these cases the waves originate or are significantly amplified at the equatorial plane and propagate down the field line, one can assume that the wave signal is present only over half the field line, starting at the equator. The self-consistency of this model has been demonstrated by *Nunn* [1974].

In most of our computations we have used a wave field that has a constant intensity over the entire field line. We have, however, computed the precipitated flux for the case of a wave which has a constant intensity over one half of the field line and negligible intensity over the other. Our result shows that the precipitated flux for the case of the half-field-line wave is not more than 20% lower than that for the full-field-line case, when the same maximum wave amplitude is assumed in each case. This is a reasonable result when one considers that particles which scatter into the loss cone generally are near the loss cone to begin with and thus have little perpendicular energy to transfer to the wave during the scattering process. Consequently, the details of the wave's amplitude and phase changes due to feedback effects generally depend almost entirely upon the higher pitch angle particles. Thus since the particles near the loss cone are effectively decoupled from the wave-particle feedback system, we would expect them to respond mainly to the gross properties of the wave (for example, average wave amplitude) rather than to the details of the feedback process. Since the gross properties of non-self-consistent full-field-line wave and the self-consistent one-half-field-line wave are similar, we then expect the precipitated fluxes to be similar also.

Acknowledgments. We wish to acknowledge the many valuable discussions we have held with our colleagues at the Radioscience Laboratory, We wish to thank M. Walt of the Lockheed Physical Sciences Laboratory for his interest and valuable comments on the paper. This research was supported by the National Aeronautics and Space Administration under contract NGL-05-020-008. The bulk of our computations were made on the CDC7600 computer of the National Center for Atmospheric Research (NCAR) in Boulder, Colorado, which we have used through a Remote Job Entry Terminal at Stanford. Our use of this facility was made possible by a Computer Resources Units grant from NCAR.

REFERENCES

Anderson, R. R., Wave particle interactions in the evening magnetosphere during geomagnetically disturbed periods, Ph.D. thesis, Univ. of Iowa, Iowa City, 1976.

Ashour-Abdalla, M., Amplification of whistler waves in the magnetosphere, *Planet. Space Sci., 20,* 639, 1972.

Bell, T. F., Wave particle gyroresonance interactions in the earth's outer ionosphere, *Tech. Rep. 3412-5,* Radiosci. Lab., Stanford Electron. Lab., Stanford Univ., Stanford, Calif., 1964.

Bell, T. F., Nonlinear Alfvén waves in a Vlasov plasma, *Phys. Fluids, 8,* 1829, 1965.

Bell, T. F., ULF wave generation through particle precipitation induced by VLF transmitters, *J. Geophys. Res., 81,* 3316, 1976.

Bell, T. F., and O. Buneman, Plasma instability in the whistler mode caused by a gyrating electron stream, *Phys. Rev., Ser. A, 133,* 1300, 1964.

Brice, N., Fundamentals of VLF emission generation mechanisms, *J. Geophys. Res., 69,* 4515, 1964.

Brinca, A. L., Whistler sideband growth due to nonlinear wave-particle interaction, *J. Geophys. Res., 77,* 3508, 1972.

Bud'ko, N. I., V. I. Karpman, and O. A. Pokhstelov, Nonlinear theory of the monochromatic circularly polarized VLF and ULF waves in the magnetosphere, *Cosmic Electrodynamics, 3,* 147, 1972.

Burtis, W. J., and R. A. Helliwell, Magnetospheric chorus: Occurrence patterns and normalized frequency, *Planet. Space Sci., 24,* 1007, 1976.

Crystal, T., Nonlinear currents stimulated by monochromatic whistler mode (WM) waves in the magnetosphere, *Tech. Rep. 3465-4*, Radiosci. Lab. Stanford Electron. Lab., Stanford Univ., Stanford, Calif., 1975.

Das, A. C., A mechanism for VLF emissions, *J. Geophys. Res., 76*, 6915, 1971.

Dungey, J. W., Loss of Van Allen electrons due to whistlers, *Planet. Space Sci., 11*, 591, 1963.

Dungey, J. W., Effects of electromagnetic perturbations on particles trapped in the radiation belts, *Space Sci. Rev., 4*, 199, 1964.

Dysthe, K. B., Some studies of triggered whistler emissions, *J. Geophys. Res., 76*, 6915, 1971.

Gendrin, R., Pitch angle diffusion of low energy protons due to gyroresonant interaction with hydromagnetic waves, *J. Atmos. Terr. Phys., 30*, 1313, 1968.

Gendrin, R., Phase bunching and other non-linear processes occurring in gyroresonant wave-particle interactions, *Astrophys. Space Sci., 28*, 245, 1974.

Gurnett, D. A., and L. A. Frank, VLF hiss and related plasma observations in the polar magnetosphere, *J. Geophys. Res., 77*, 172, 1972.

Helliwell, R. A., *Whistlers and Related Ionospheric Phenomena*, Stanford University Press, Stanford, Calif., 1965.

Helliwell, R. A., A theory of discrete VLF emissions from the magnetosphere, *J. Geophys. Res., 72*, 4773, 1967.

Helliwell, R. A., Intensity of discrete VLF emissions, in *Particles and Fields in the Magnetosphere*, edited by B. M. McCormac, p. 292, D. Reidel, Hingham, Mass., 1970.

Helliwell, R. A., and T. L. Crystal, A feedback model of cyclotron interaction between whistler-mode waves and energetic electrons in the magnetosphere, *J. Geophys. Res., 78*, 7357, 1973.

Helliwell, R. A., and J. P. Katsufrakis, VLF wave-injection experiments into the magnetosphere from Siple Station, Antarctica, *J. Geophys. Res., 79*, 2571, 1974.

Helliwell, R. A., J. P. Katsufrakis, and M. L. Trimpi, Whistler-induced amplitude perturbation in VLF propagation, *J. Geophys. Res., 78*, 4679, 1973.

Helliwell, R. A., J. P. Katsufrakis, T. F. Bell, and R. Raghuram, VLF line radiation in the earth's magnetosphere and its association with power system radiation, *J. Geophys. Res., 80*, 4249, 1975.

Heyborne, R. L., Observations of whistler mode signals in the Ogo satellites from VLF ground station transmitters, *Tech. Rep. 3415/3418-1*, Radiosci. Lab., Stanford Electron. Lab., Stanford Univ., Stanford, Calif., 1966.

Inan, U. S., Nonlinear gyroresonant interactions of energetic particles and coherent VLF waves in the magnetosphere, *Tech. Rep. 3414-3*, Radiosci. Lab., Stanford Electron. Lab., Stanford Univ., Stanford, Calif., 1977.

Inan, U. S., T. F. Bell, D. L. Carpenter, and R. R. Anderson, Explorer 45 and Imp 6 observations in the magnetosphere of injected waves from the Siple Station VLF transmitter, *J. Geophys. Res., 82*, 1177, 1977.

Karpman, V. I., Ja. N. Istomin, and D. R. Shklyar, Nonlinear frequency shift and self-modulation of the quasi-monochromatic whistlers in the inhomogeneous plasma (magnetosphere), *Planet. Space Sci., 22*, 859, 1974*a*.

Karpman, V. I., Ja. N. Istomin, and D. R. Shklyar, Nonlinear theory of a quasi-monochromatic whistler mode wave packet in inhomogeneous plasma, *Plasma Phys., 16*, 685, 1974*b*.

Kennel, C. F., Consequences of a magnetospheric plasma, *Rev. Geophys. Space Phys., 7*, 379, 1969.

Kennel, C. F., and F. Engelmann, Velocity space diffusion from weak plasma turbulence in a magnetic field, *Phys. Fluids, 9*, 2377, 1966.

Kennel, C. F., and H. E. Petschek, Limit on stably trapped particle fluxes, *J. Geophys. Res., 71*, 1, 1966.

Laaspere, T., and R. A. Hoffman, New results on the correlation between low-energy electrons and auroral hiss, *J. Geophys. Res., 81*, 524, 1976.

Lyons, L. R., Comments on pitch-angle diffusion in the radiation belts, *J. Geophys. Res., 78*, 6793, 1973.

Lyons, L. R., General relations for particle diffusion in pitch angle and energy, *J. Plasma Phys., 12*, 45, 1974*a*.

Lyons, L. R., Pitch angle and energy diffusion coefficients from resonant interactions with ion-cyclotron and whistler waves, *J. Plasma Phys., 12*, 417, 1974*b*.

Lyons, L. R., and D. J. Williams, The quiet time structure of energetic (35–560 keV) radiation belt electrons, *J. Geophys. Res., 80*, 943, 1975.

Lyons, L. R., R. M. Thorne, and C. F. Kennel, Electron pitch-angle diffusion driven by oblique whistler mode turbulence, *J. Plasma Phys., 6*, 589, 1971.

Lyons, L. R., R. M. Thorne, and C. F. Kennel, Pitch-angle diffusion of radiation belt electrons within the plasmasphere, *J. Geophys. Res., 77*, 3455, 1972.

Matsumoto, H., Theoretical studies on whistler mode wave particle interactions in the magnetosphere plasma, Ph.D. thesis, Kyoto Univ., Kyoto, Japan, 1972.

Muzzio, J. L. R., ELF propagation in the plasmasphere based on satellite observations of discrete and continuous forms, *Tech. Rep. 3439-2*, Radiosci. Lab., Stanford Electron. Lab., Stanford University, Stanford, Calif., 1971.

Nunn, D., A theory of VLF emissions, *Planet. Space Sci., 19*, 1141, 1971.

Nunn, D., A self-consistent theory of triggered VLF emissions, *Planet. Space Sci., 22*, 349, 1974.

Palmadesso, G., and G. Schmidt, Collisionless damping of a large amplitude whistler wave, *Phys. Fluids, 14*, 1411, 1971.

Palmadesso, G., and G. Schmidt, Stability of a steady, large amplitude whistler wave, *Phys. Fluids, 15*, 485, 1972.

Park, C. G., The role of man-made VLF signals and noise in wave-particle interactions in the magnetosphere, in *Physics of Solar Planetary Environments*, edited by D. J. Williams, AGU, Washington, D. C., 1976.

Roberts, C. S., Electron loss from the Van Allen zones due to pitch angle scattering by electromagnetic disturbances, in *Radiation Trapped in the Earth's Magnetic Field*, edited by B. M. McCormac, pp. 403, 421, D. Reidel, Hingham, Mass., 1966.

Roberts, C. S., Cyclotron resonance and bounce resonance scattering of electrons trapped in the earth's magnetic field, in *Earth's Particles and Fields*, edited by B. M. McCormac, pp. 317–336, Reinhold, New York, 1968.

Roberts, C. S., Pitch angle diffusion of electrons in the magnetosphere, *Rev. Geophys. Space Phys., 7*, 305, 1969.

Roederer, J. G., *Dynamics of Geomagnetically Trapped Particles*, Springer, New York, 1970.

Rosenberg, T. J., R. A. Helliwell, and J. P. Katsufrakis, Electron precipitation associated with discrete very-low-frequency emissions, *J. Geophys. Res., 76*, 8445, 1971.

Roux, A., and R. Pellat, A study of triggered emissions, in *Magnetospheric Particles and Fields*, edited by B. M. McCormac, p. 209, D. Reidel, Hingham, Mass., 1976.

Schield, M. A., and L. A. Frank, Electron observations between the inner edge of the plasma sheet and the plasmasphere, *J. Geophys. Res., 75*, 5401, 1970.

Schulz, M., and L. J. Lanzerotti, *Particle Diffusion in the Radiation Belts*, Springer, New York, 1973.

Stiles, G. S., and R. A. Helliwell, Frequency time behavior of artificially stimulated VLF emissions, *J. Geophys. Res., 80*, 608, 1975.

Taylor, W. W. L., and D. A. Gurnett, Morphology of VLF emissions observed with the Injun 3 satellite, *J. Geophys. Res., 73*, 5615, 1968.

Thorne, R. M., E. J. Smith, R. K. Burton, and R. E. Holzer, Plasmaspheric hiss, *J. Geophys. Res., 78*, 1581, 1973.

Tsurutani, B. T., and E. J. Smith, Postmidnight chorus: A substorm phenomenon, *J. Geophys. Res., 79*, 118, 1974.

Wang, T. N. C., and T. F. Bell, VLF/ELF radiation patterns of arbitrarily oriented electric and magnetic dipoles in a cold lossless multicomponent magnetoplasma, *J. Geophys. Res., 77*, 1174, 1972.

(Received April 7, 1977;
accepted January 19, 1978.)